For Table of Contents Use Only

Factors Defining the Effects of Macromolecular Crowding on Dynamics and Thermodynamic Stability of Heme Proteins *In-vitro*

Rajesh Kumar[‡], Deepak Sharma[†], Vinay Kumar[□] and Rajesh Kumar*[††‡]

[††]Centre for Chemical Sciences, School of Bassic and Applied Sciences, Central University of Punjab, Bathinda, 151001, India

[‡]School of Chemistry and Biochemistry, Thapar University, Patiala 147004, India

[†]Council of Scientific and Industrial Research—Institute of Microbial Technology, Sector 39A, Chandigarh, India

[□]Centre for Plant Sciences, School of Bassic and Applied Sciences, Central University of Punjab, Bathinda, 151001, India

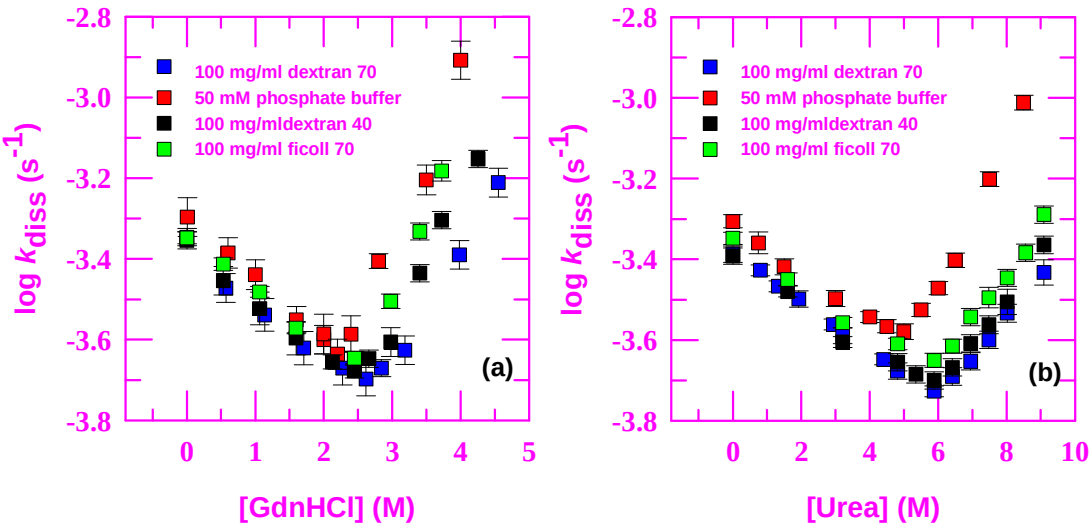

Factors Defining the Effects of Macromolecular Crowding on Dynamics and Thermodynamic Stability of Heme Proteins *In-vitro*

Authors:

Rajesh Kumar[‡], Deepak Sharma[†], Vinay Kumar[□] and Rajesh Kumar*[††‡]

Authors' Addresses:

[††] Department of Chemical Sciences, School of Bassic and Applied Sciences, Central University of Punjab, Bathinda, 151001, India

[‡]School of Chemistry and Biochemistry, Thapar University, Patiala 147004, India

[†]Council of Scientific and Industrial Research—Institute of Microbial Technology, Sector 39A, Chandigarh, India

[□] Department of Plant Sciences, School of Bassic and Applied Sciences, Central University of Punjab, Bathinda, 151001, India

Corresponding Authors at:

Department of Chemical Sciences, School of Bassic and Applied Sciences,

Central University of Punjab, Bathinda, 151001, India

School of Chemistry and Biochemistry, Thapar Institute of Enginnering and Technology University

Patiala, 147004, India

Email: rajeshchem01@gmail.com

Phone: 91-164-286-4255

Abstract

The role of crowding agents on structure and activities of heme proteins has been established. Analysis of kinetic and thermodynamic parameters measured for CO-dissociation reaction of natively-folded carbonmonoxycytochrome *c* (NCO) and carbonmonoxymyoglobin (MbCO) at different [GdnHCl] or [Urea] in the presence of crowding agents (dextran 40,dextran 70 and ficoll 70) demonstrate that (i) at low denaturant concentrations, crowder presence enhances the denaturant-mediated restricted dynamics of NCO and MbCO, and (ii) at higher denaturant concentrations, large scale unfolding-fluctuations dominate the dynamics and inclusion of crowder counteracts the structural-fluctuations causing the unfolding of proteins. Thermodynamic analysis of thermal and urea-unfolding curves of cytochrome *c* (Cyt *c*) and myoglobin (Mb) measured at different [GdnHCl] in presence of crowding agents reveals that crowder presence counterbalances and strengthens the destabilizing action of GdnHCl on stability of Cyt *c* and Mb, respectively. This study further demonstrates that the size, shape and concentration of crowding agent modulate the effect of crowder on denaturant-mediated dynamics and thermodynamic stability of heme proteins.

Keywords: Crowding agents; constrained dynamics; thermodynamic stability; counteracting effect; excluded volume effect

1. Introduction

The interface of protein structure and protein biophysics is mostly investigated in *in-vitro* condition with diluted aqueous environment. However, proteins synthesis and its associated processes such as protein folding, enzyme activity, structural allostery *etc*. occur in *in-vivo* conditions of crowded cellular environment. The intracellular environment, offers an extremely crowded milieu that influences protein structure and biophysics [1-3]. It has been estimated that the concentration of macromolecules in the cytoplasm is in the range of 80 to 400 mg ml^{-1}[4-5]. About 10 to 40% of cellular volume is occupied by different macromolecules [6-7]. The fraction of available intracellular volume for other macromolecules depends on the concentration, size and shape of different biomolecules present in each compartment and with limited amount of free water. The crowded environment influences excluded volume effects, probability of nonspecific intermolecular interactions, and solvent viscosity. In previous reports, the influence of crowding effects was explained by two different theories, hardcore repulsions and soft (*i.e.*, chemical) interactions [8]. In hardcore repulsion, crowding reduces the available space and induces the compactness of protein being studied. However, hardcore repulsive effect considers only the arrangement of molecules, and avoids their interaction with proteins. In addition, it improves protein stability by decreasing the entropy of unfolding [9-12]. On the other hand, the soft or chemical interactions can be either attractive or repulsive. In case of attractive interactions, the nonspecific binding of cosolutes with protein backbone leads to a preferential exclusion of the osmolytes or crowders from the protein surface and results into a preferential hydration of proteins [13]. As the solvent accessible surface area of the unfolded state of protein increases, the folding equilibrium shifts towards the native state [12, 14-15].

A high concentration of selected polymers serves as “crowding agents”. A number of studies have also been carried out under these conditions to assess the effect of molecular crowding on protein structure and function [16-59]. Sasahara *et al*. (2003) showed that high concentration of smaller crowder dextran 35 forced the acid-denatured cytochrome *c* (Cyt *c*) to a near-native molten globule state [16]. In addition, a number of reports have demonstrated the influence of crowders on the functional properties of proteins or enzymes [60-70]. Dhar *et al*. (2010) documented the enhanced activity of phosphoglycerate kinase (PGK) by more than ten folds upon macromolecular crowding [17]. Aoki *et al*. (2011) proposed quasi-processive phosphorylation of ERK under the physiological state of molecular crowding [18]. Similarly, remarkable changes in the diffusional behavior of intracellular proteins and molecular properties of motor proteins, kinesins were also documented [19-21]. In addition, potential role of crowding agents has also been reported for human diseases associated with protein aggregation and fibril formation such as various neurodegenerative disorders [22-29]. A number of reports demonstrated that crowding agents also influence the stability and structural content of folded and unfolded proteins [3, 30-36, 71-73]. Chen *et al.* (2012) assessed the effect of macromolecular crowding on burst phase kinetics of cytochrome *c* folding [74]. Pioneering works by Wittung-Stafshede group evaluated the effect of crowding agents on the denaturant-dependent thermal stability of ferricytochrome *c* (Ferricyt *c*) [71]. They demonstrated that the size, shape and concentration of synthetic crowding agents modulate the GdnHCl-dependent thermal stability of native Ferricyt *c*.

Although the effect of crowding agents on fast protein dynamics that control conformational transitions linked with protein function has been studied [73-77], the effects of crowding agents on slow changes in structural dynamics of proteins across the folding-unfolding transition are not explored so far. An understanding of the slow changes in structural fluctuations in folding can be

achieved by measuring the alterations in thermal fluctuations at both atomic and large-scale collective level [78-81]. Though the role of crowding agents on thermal fluctuations of Ω-loop of NCO has been investigated [78], the role of crowding agents on structural fluctuations of MbCO is not explored so far.

In present work, the roles of variations of size, shape, and concentration of crowding agent on the denaturant-dependent structural dynamics of NCO and MbCO were evaluated by measuring the rates of CO dissociation from NCO [78] and MbCO [82] in the absence and presence of 50-200 mg ml^{-1} crowder of varying sizes (dextran 40 and dextran 70) and shape (dextran 70 and ficoll 70) under variable concentrations of denaturants (urea and GdnHCl). In addition, the roles of variations of crowding agents were also evaluated on denaturant-dependent stability of heme proteins by analyzing the thermal and chemical denaturation curves of Cyt *c* and Mb at fixed concentrations of crowding agents (dextran 40, dextran 70 and ficoll 70) under variable concentrations of denaturants. These results revealed that (i) at lower denaturant concentration, crowder potentiates the denaturant-mediated constrained dynamics of NCO and MbCO but at higher denaturant concentrations it opposes the structural fluctuation causing the unfolding of protein, and (ii) the size, shape and concentrations of crowding agents modulate the effect of crowder on denaturant-dependent dynamics and thermodynamic stability of heme proteins.

2. Materials and Methods

Proteins (Horse heart Cyt *c* (type VI) and horse heart Mb), crowding agents (dextran 40, dextran 70 and Ficoll 70) and salt of buffer (NaH_2PO_4 and Na_2HPO_4) were purchased from Sigma-Aldrich. Denaturants, GdnHCl and urea of ultra pure grade were purchased from USB. All others chemicals

were of analytical grade. All experiments were performed in 0.1 M sodium phosphate buffer at pH 7. The experiments for reduced form of heme proteins were carried out under strictly anaerobic conditions. The kinetics and thermodynamic data were analyzed with the program Sigma Plot (v. 11). Concentrations of Ferrocytochrome *c* (Ferrocyt *c*), Ferricyt *c* and Mb were measured using absorption coefficient, 28000 M^{-1} cm^{-1} for Ferrocyt *c* at 550, 106000 M^{-1} cm^{-1} for Ferricyt *c* at 410 nm, and 171000 M^{-1} cm^{-1} for Mb at 409 nm.

2.1. Kinetics of thermally-driven CO-dissociation of NCO at different concentrations of denaturant in the presence of crowding agent

Unfolded Ferricyt *c* was prepared in 6.5 M GdnHCl, deaerated by passing dry N_2 gas and further reduced by ~3.0 mM of sodium dithionite solution. The stock solution of sodium dithionite was prepared in a sleeved rubber stoppers glass tube by dissolving 120 mg of solid sodium dithionite in 1.0 mL of deaerated phosphate buffer, pH 7.0 under dry N_2 atmosphere. The unfolded Ferrocyt *c* represented as "U" thus obtained was liganded with CO by passing the dry CO gas through the protein solution under dry N_2 atmosphere. To determine the effect of crowding agents on denaturant-dependent dynamics of Ferrocyt *c*, CO-liganded unfolded Ferrocyt *c* (UCO) was diluted 101-fold into a degassed and dithionite-reduced CO-free refolding buffer with series of dilution of denaturants (GdnHCl and urea) in the absence and presence of 50-200 mg ml^{-1}crowder (dextran 70, dextran 40 and ficoll 70) at pH 7. This approach facilitates the conversion of UCO-state to NCO-state. In the stopped-flow experiment, when denaturant is diluted out into a CO-free refolding buffer, the UCO-state collapses to a native-like compact state (NCO-state) within 3.5 ms (k = 305 s^{-1} at pH 7, 22 °C), where the non-native Fe^{2+}-CO contact persists [80]. Recently, the

NCO-state was characterized using various spectroscopic techniques (near and far-UV CD, tryptophan (Trp) fluorescence and ^{1}H NMR) and found that the NCO-state exhibits the generic properties of molten globules [78]. The comparison of the far-UV CD spectra of N-state, UCO-state and NCO-state shows that upon refolding of UCO state to NCO-state, the NCO-state acquires the native-like secondary structure (Fig. S1).

The slow thermally-driven CO dissociation kinetics (NCO → N+CO) was monitored by absorbance of heme (pH 7, 22°C) at 550 nm on Shimadzu 2450 spectrophotometer coupled with S-1700 thermoelectric system. The final concentration of protein was ~7 µM. The kinetic data were analyzed by nonlinear least squares fit to a single-exponential rate expression.

2.2 Kinetics of CO dissociation of MbCO by hexacyanoferrate ion at different concentrations of denaturant in the presence of crowding agent

CO dissociation from MbCO was carried out by CO-replacement of MbCO by hexacyanoferrate ion (MbCO + CN^{-} → MbCN + CO) [82] at pH 7.0, 22 °C. Briefly, Mb (~1 mM) initially dissolved in phosphate buffer (pH 7.0) and afterward deaerated and reduced by the addition of sodium dithionite (final concentration ~0.5 mM). The reduced Mb was then liganded with CO under dry N_2 atmosphere, by passing a slow stream of dry CO gas. To determine the effect of crowding agents on structural dynamics of Mb, ~25 µl of CO-liganded protein (MbCO) was added into 2.0 ml solution of potassium hexacyanoferrate containing a desired concentration of the crowding agent. In order to evaluate the effect of crowding agents on denaturant-dependent dynamics of Mb, CO dissociation from MbCO was also carried out under variable concentration of GdnHCl at fixed concentration of crowding agent (dextran 70, dextran 40 and ficoll 70), pH 7, 22 °C. The change in the absorbance of

the reaction medium was monitored at 421 nm on Shimadzu (UV-2450) spectrophotometer at 22°C. The final concentrations of protein and hexacyanoferrate ion are 12 and 500 μM, respectively.

2.3. Activation thermodynamic parameters for CO dissociation kinetics of NCO at different concentrations of denaturant in the presence of crowding agent

To evaluate the effect of crowding agents on denaturant-dependent activation thermodynamic parameters (activation enthalpy ($\Delta H_{diss}^{\ddagger}$) and activation entropy ($\Delta S_{diss}^{\ddagger}$)), the temperature dependent rate profile for CO-dissociation of NCO, recorded under variable concentrations of denaturant (urea and GdnHCl) in the absence and presence of fixed concentration of crowding agent (dextran 70, dextran 40 and ficoll 70) was analyzed using Eyring equation (1) [78],

$$\ln(k_{diss}h/k_B T) = (\Delta S_{diss}^{\ddagger}/R) - (\Delta H_{diss/}^{\ddagger}/RT) \qquad (1)$$

where 'k_B' is the Boltzmann constant, 'h' is the Planck constant, 'R' is the gas constant, k_{diss} is the thermally-driven CO dissociation rate constant of NCO, and $\Delta H_{diss}^{\ddagger}$ and $\Delta S_{diss}^{\ddagger}$ are changes in activation enthalpy and activation entropy, respectively for CO-dissociation reaction of NCO-state.

2.4 Effect of crowding agents on the denaturant-dependent far-UV CD spectra of heme proteins

To determine the effect of crowding agents on the denaturant-dependent far-UV CD spectra of heme proteins, the Far-UV CD (200-250 nm, 1.0 mm cell) spectra of Ferricyt *c* and Mb were

collected under variable concentrations of denaturants in the presence of 200 mg ml^{-1} crowder (dextran 70, dextran 40, ficoll 70) at pH 7, 25 °C on JASCO 815 spectropolarimeter coupled with PTC 424S/15 peltier system (-10-110 °C). The CD spectra of these proteins were normalized by subtracting the CD spectra of the corresponding blank solutions of same concentration of different crowding agents at pH 7.0, 25 °C. The final concentrations of Ferricyt *c* and Mb were 15 μM and 12 μM, respectively.

2.5 Effect of crowding agents on the denaturant-dependent thermal denaturations of heme proteins

To determine the effect of crowding agents on denaturant-dependent thermal denaturation of heme proteins, the visible absorbance and far-UV CD-monitored thermal denaturation profiles of Ferrocyt *c* (Abs at 550 nm, 416 nm and CD at 222 nm) and Mb (Abs at 409 nm and CD at 222 nm) were collected under variable concentrations of denaturant (urea and GdnHCl) in the absence and presence of ~100, 200 and 300 mg ml^{-1} crowder (dextran 40, dextran 70 and ficoll 70) at pH 7.0 The pathlength of the cuvettes used for visible absorbance and far-UV CD were 10 mm and 1.0 mm, respectively. The absorbance (409 nm, 416 nm and 550 nm) monitored melting data were collected on Shimadzu (UV-2450) spectrophotometer coupled with S-1700 thermoelectric system (0-110 °C). The Far-UV CD (222 nm) monitored melting data were collected on JASCO 815 CD-spectrophotometer coupled with PTC 424S/15 system (-10-110 °C). The temperature ranges were 25 to 110 °C for Ferrocyt *c* and 25 to 90 °C for Mb. The final protein concentrations for absorbance and CD monitored thermal denaturation curves were ~5.0 μM and ~12 μM, respectively. The dithionite concentrations were ~3 mM and ~1 mM for visible absorbance (550 nm) and far-UV CD (222 nm) monitored thermal unfolding measurements of Ferrocyt *c*,

respectively. The peltier-controlled heating rates in far-UV CD and visible absorbance-monitored thermal denaturation of heme proteins were 1.0 and 2.0 °C/min., respectively. By assuming a two-state denaturation process, the thermal denaturation data were analyzed by equation (2) [82, 85],

$$y(T) = \frac{(y_F + m_F T) + (y_U + m_U T)\exp\left(\frac{\Delta H_m\left(\frac{T}{T_m} - 1\right) - \Delta C_p\left(T_m - T + T\ln\left(\frac{T}{T_m}\right)\right)}{RT}\right)}{1 + \exp\left(\frac{\Delta H_m\left(\frac{T}{T_m} - 1\right) - \Delta C_p\left(T_m - T + T\ln\left(\frac{T}{T_m}\right)\right)}{RT}\right)} \quad (2)$$

where y(T) is the observed variable parameters (ε_{550nm}, ε_{409nm}, and $CD_{222\ nm}$), y_F and y_D and m_F and m_D, represent intercepts and slopes of the folded and unfolded baselines, respectively; T, absolute temperature; ΔC_p denotes heat capacity change, R, gas constant, and ΔH_m represent the van't Hoff enthalpy at thermal denaturation midpoint (T_m).

2.6. Effect of crowding agents on the GdnHCl-dependent urea-induced-unfolding of heme proteins

To determine the effect of crowding agents on the GdnHCl-dependent urea-induced unfolding of heme proteins, the Trp fluorescence (ex: 280 and em: 340 nm) monitored urea-induced unfolding curves of Ferricyt *c* and Mb were measured under variable concentrations of GdnHCl in the absence and presence of 100 mg ml^{-1} crowder (dextran 40 and 70 and ficoll 70) at pH 7.0, 25ºC. For these measurements, the fluorescence emission spectra (ex: 280 nm, em: 310-390 nm) of Ferricyt *c* and Mb samples were collected on Perkin Elmer LS-55 fluorescence spectrophotometer or The PTI QM 40 (Photon Technology). The final concentration of protein was ~8 μM. In aqueous

solution, urea forms cyanate, which can carbamylate lysyl epsilon-amino groups and changes the electrostatic properties of studied proteins. The presence of cyanate in solution could lead to modification of studied proteins prior to or during data collection. Therefore, to prevent the cyanate formation, the experiment must be preceded within 3 hrs. The concentrations of the urea and GdnHCl solutions before and after the experiments were determined based upon the refractive index measurements by Thermo Scientific refractometer. The data were fitted to a standard two-state equilibrium unfolding represented as equation (3) [86],

$$Y_{obs} = \frac{(C_N + M_N[D]) + (C_U + M_U[D])exp\left[\frac{-\Delta G_D + m_g[D]}{RT}\right]}{1 + exp\left[\frac{-\Delta G_D + m_g[D]}{RT}\right]} \quad (3)$$

where, Y_{obs} parameter represents as observed signal, and C_N and C_U, and M_N and M_U represent intercepts and slopes of native and unfolded baselines, respectively, [D] is the concentration of denaturant in M, R is the gas constant, ΔG_D, the free energy associated with the transition, and m_g, the surface area of the protein exposed by the solvent. C_m, the transition mid-point of denaturant concentration, was calculated as $C_m = \Delta G_D/m_g$.

2.7 Denaturants concentration corrections due solvent excluded volume

It has been established that the synthetic crowders may not interact with any solute molecules and increases the concentration of any small solute by decreasing its available volume through steric repulsion phenomena [87-88]. The denaturants concentrations in the protein samples were thus corrected ($[denaturant]_{corr}$) to account for the solvent-excluded volume due to the presence of crowder. For this, Christiansen *et al* estimated the partial specific volume ($\bar{v}_t$) value

~0.65±0.02 ml/g for ficoll 70, dextran 40 and dextran 70 [89]. The $\bar{v}_t$ value was found to be independent on the amount of crowding agent and same in buffer as well as in low to high denaturant concentrations, suggesting that there is no specific interaction between denaturant (GdnHCl/urea) with crowding agent (ficoll/dextran) [89]. For denaturants concentration correction, following equation was used [71, 89],

$$[Denaturants]_{corr} = (1/f_{av})[Denatrants] \quad (4)$$

where, f_{av} represents the volume fraction available for the solvent and which can be estimated as [71, 86]:

$$f_{av} = (1 - \bar{v}_t [Crowding\ agent](\text{g/ml})) \quad (4a)$$

For example, the value of f_{av} for 200 mg ml^{-1} ficoll 70 is ~ 0.87 (i.e., 1-(0.65ml/g)×(0.2g/mL)). All selected denaturants concentrations used for kinetic and stability experiments were corrected in the same way on the basis of the concentration of present crowding agent (s).

3.0 Results and Discussion

3.1 Size and shape of crowding agents control the dynamics of MbCO and NCO

CO dissociation from MbCO leads to a significant decrease in the absorbance at Soret region ~421nm [82]. The representative CO-dissociation kinetic profiles of MbCO recorded at 22°C, pH 7 is shown in Fig.1a. The kinetic data in Fig. 1a are best fitted to single-exponential rate expression with CO-dissociation rate constant, k_{diss} ~0.032 s^{-1}. To investigate the role of crowding agents on dynamics of MbCO, the rate constant of CO dissociation of MbCO (k_{diss}) was measured at

different concentration of crowder (dextran 40, dextran 70 and ficoll 70) at pH 7.0, 22 °C. Fig. 1b shows the variations of log k_{diss} for MbCO with increase of [Crowding agent]. As [Crowding agent] is increased, log k_{diss} decreases exponentially (Fig. 1b) which reveals that the crowder presence retards the CO dissociation and thus restricts the dynamics of protein. Furthermore, the crowder-mediated retardation in CO dissociation for MbCO typically follows the order, dextran 70 > dextran 40 > ficoll 70. Recent, CO dissociation kinetic studies of NCO carried out in the presence of different concentrations of crowding agent (dextran 40, dextran 70, ficoll 70) also revealed that the crowder-mediated retardation for NCO typically follows the order, dextran 70 > dextran 40 > ficoll 70) [78]. Thus, the effect of crowding on CO dissociation kinetics of NCO and MbCO follows the same trend. As dextran 70 has larger size than dextran 40 [71] and different shape than ficoll 70 [71], the results indicate that size and shape of crowding agents play vital roles in controlling the dynamics of MbCO and NCO. The larger sized dextran has been reported to contribute significantly to caging or confinement environment, and therefore plays important roles in controlling the dynamics of proteins [90].

3.2 Size and shape of crowding agent modulate the effect of crowding on denaturant-dependent motional dynamics of NCO and MbCO

Thermal dissociation of CO from NCO-state leads a significant increase in the absorbance of α-band (550 nm) [78, 84]. The representative CO-dissociation kinetic profiles of NCO recorded in the presence of 0.05 M GdnHCl at 22°C, pH 7 is best fitted to single exponential rate expression with thermally-driven CO dissociation rate constant, k_{diss} ~5.5 $\times 10^{-4}$ s^{-1} (Fig. S1). The thermally-driven CO dissociation from NCO (Fe^{2+}-CO + M80→ Fe^{2+}- M80 + CO) is not a global probe of

dynamics but rather it is a low-frequency local motion that controls the structural fluctuation of M80-containing Ω-loop [84, 91-92]. This is presumably due to two main reasons, (i) the neighboring residues of M80 have high thermal factors [93], and (ii) the local mobility of the heme ring is suppressed by the intrinsic size and the rigidity of the ring system [94]. Thus the cosolute (crowder or denaturant) modulation of k_{diss} describes the manner by which the collective motion of M80-containing Ω-loop responds to cosolute environment in the reaction medium.

To investigate the role of crowding agents on the denaturant-dependent structural fluctuation of NCO and MbCO, the k_{diss} for NCO and MbCO were measured under variable concentrations of denaturant at fixed concentration of crowding agent (dextran 40, dextran 70 and ficoll 70). Fig. 2a and Fig. 2b present the denaturant-dependence of log k_{diss} for NCO measured in the absence and presence of ~50, 100, 200 mg ml^{-1} dextran 70 (Fig. 2a) and ficoll 70 (Fig. 2b). The denaturant-dependence of log k_{diss} for NCO measured in the presence of ~100 mg ml^{-1} crowder (dextran 40, dextran 70 and ficoll 70) is shown in Fig. 2c. Fig. 2d presents the denaturant-dependence of log k_{diss} for MbCO measured in the absence and presence of ~200 mg ml^{-1} crowder (dextran 40, dextran 70 and ficoll 70) at pH 7.0, 22 °C.

Both in the absence and presence of crowding agents, as denaturant concentration is increased starting from strongly native-like conditions, log k_{diss} initially decreases and then increases, displaying minimum around 2.0-2.4 M GdnHCl and 5.0-5.5 M urea for NCO (Figs. 2a-2c) and 0.1-0.2 M GdnHCl for MbCO (Fig. 2d). At low denaturant concentrations, the denaturant ions can stabilize and compact the proteins by screening the protein charges electrostatically [85, 95-99]. Analysis of ITC and X-ray data has shown evidences for direct interactions between protein groups and guanidinium ion or urea molecule [100-102]. At lower concentrations, guanidinium ion or urea molecule can interact with a protein molecule through multiple hydrogen bonds and van der Waals

interactions [101-102]. A recent intermolecular docking study performed between the Ferrocyt *c* and denaturant (urea, GdnHCl) revealed that about seven urea molecules form multiple variable length hydrogen bonds with the backbone–backbone or backbone–side chain atoms of the Ω-loop of Cyt *c* [103]. Such denaturant mediated nonspecific polyfunctional interactions may compact the protein and also reduce the motional freedom and internal motions of the native proteins [82,84,92, 101-103]. Thus, the initial decrease of log k_{diss} around 2.0-2.4 M GdnHCl and 5.0-5.5 M urea for NCO (Figs. 2a-2c) and 0.1-0.2 M GdnHCl for MbCO (Fig. 2d), indicates that the subdenaturing concentrations of denaturants reduce the level of structural fluctuations responsible for CO dissociation from NCO and MbCO.

Crowding agents and subdenaturing concentrations of denaturants were found to decrease the rate of CO dissociation reaction (Fig. 1b and Figs. 2a,2b,2d), therefore, the inclusion of crowding agent at subdenaturing concentrations of denaturants could enhance the denaturant-mediated decrease in the rate of CO dissociation. As the concentration of crowding agent is increased from 0 to 200 mg ml^{-1}, the rate-denaturant profile shifted vertically down to lower k_{diss} (Fig. 2a,2b,2d). A slight horizontal shift toward higher concentration of denaturant is also observed (Figs. 2a and 2b). The crowding-mediated vertical and slight horizontal shifts in the rate-denaturant profile revealed that crowder presence potentiates the denaturant-mediated restricted dynamics of protein. Within the subdenaturing region, the effect of crowding agent on decrease in log k_{diss} typically follows the order: dextran 70 > dextran 40 > ficoll 70 (Figs. 2c and 2d), indicating that the size and shape of crowder control denaturant-mediated constrained dynamics of protein. Previous simulation studies have also supported the similar observations [3, 73, 90].

At relatively higher denaturant concentrations, the subdenaturing concentration mediated reduction in structural fluctuations is subdued by the chaotropic action of the denaturant which

unfolds and expands the protein. Thus, in the denaturing region, the increase in log k_{diss} (Figs. 2a-2d) can be attributed to protein destabilization and structural unfolding action of denaturant that subsequently facilitates the CO dissociation from NCO and MbCO. Within the denaturing region, the crowder presence opposes the denaturant-mediated increase in log k_{diss} (Figs. 2a,2b,2d). This finding reveals that the presence of crowder counteracts the structural fluctuation leading to unfolding of the protein. Within the denaturing region, the opposing effect of crowding agent on increase in log k_{diss} typically follows the order: dextran 70 > dextran 40 > ficoll 70 (Figs. 2a,2b,2d), indicating that the size and shape of crowder control the counteracting effect of crowding agent on denaturant-mediated structural-fluctuations accountable for unfolding of the protein.

3.3 Size and shape of crowding agent modulate the effect of crowding on denaturant-dependent activation thermodynamic parameter of CO-dissociation reaction of NCO

To further examine the role of size and shape of crowding agents on denaturant-dependent dynamics of NCO, the temperature dependent CO dissociation kinetics profiles of NCO were measured at various concentrations of denaturant (urea and GdnHCl) in the absence and presence of fixed concentration of crowding agent (dextran 40, dextran 70 and ficoll 70). Fig. 3a and Fig. 3b present the Eyring plots for CO-dissociation reaction of NCO at ~0.0, ~2.3 and ~4.0 M GdnHCl; and ~0.0, ~5.5 and ~8.5 M urea, respectively, in the absence and presence of 100 mg ml^{-1} crowding agent (dextran 40, dextran 70 and ficoll 70). Thermodynamic parameters *viz*; activation enthalpy (ΔH_{diss}) and activation entropy (ΔS_{diss}) for CO dissociation reaction of NCO were derived from linear least-squares fitting of these plots by Eyring equation (1) (material and method section)) [78] and are summarized in Table 1. The corresponding free energy of activation ($\Delta G_{diss}^{\ddagger}$) and entropy

change ($-T\Delta S_{diss}^{\ddagger}$) were also calculated by Gibbs free energy equation ($\Delta G_{diss}^{\ddagger} = \Delta H_{diss}^{\ddagger} - T\Delta S_{diss}^{\ddagger}$) at 25 °C (Table 1). The data in Table 1 provide several important information: (i) the subdenaturing concentrations of denaturant increase the $\Delta H_{diss}^{\ddagger}$ and the presence of crowding agent enhances the denaturant-mediated increase in $\Delta H_{diss}^{\ddagger}$, (ii) within subdenaturing region, the effect of crowder on increase in $\Delta H_{diss}^{\ddagger}$ typically follows the order as, dextran 70 > dextran 40 > ficoll 70 (Figs. 3a and 3b, Table 1), indicating potential role of size and shape of crowder in strengthening the denaturant-mediated constrained dynamics of NCO, (iii) at relatively higher concentrations, denaturants decrease the $\Delta H_{diss}^{\ddagger}$ and the presence of crowding agent opposes the denaturant-mediated decrease in $\Delta H_{diss}^{\ddagger}$ (Figs. 3a and 3b, Table 1), which suggests that the crowding agent produces a counteracting effect on the denaturant-mediated structural fluctuations causing the unfolding of protein, (iv) within the denaturing region, the efficiency of the counteracting effect on decrease in $\Delta H_{diss}^{\ddagger}$ typically follows the order as dextran 70 > dextran 40 > ficoll 70 (Figs. 2a,2b,2c and Figs. 3a and 3b,Table 1), suggesting that size and shape of crowding agent play vital roles in counteracting effect of crowder on denaturant-mediated structural fluctuation causing the unfolding of protein, and (iv) crowding-mediated increase in $\Delta H_{diss}^{\ddagger}$ was found to be accompanied by a decrease in the entropy change, $-T\Delta S_{diss}^{\ddagger}$.

3.4 Crowding agent presence does not affect the secondary structures of native- and denatured Ferricyt c and Mb

The negative Cotton effects at 210 nm and 222 nm in far-UV CD spectrum (200-250 nm) of native protein reflect the secondary structure of protein [78]. Fig. 4a and Fig. 4b present the far-UV CD spectra of Ferricyt *c* and Mb, respectively recorded in the absence and presence of 200 mg ml^{-1}

crowding agent (dextran 40, dextran 70 and ficoll 70) with urea (2.0 and 9.0 M) at pH 7.0, 25 °C. These results demonstrate that the presence of crowding agent do not greatly affect the secondary structure content of native and denatured states of Ferricyt *c* and Mb at pH 7.0, 25 °C. Two previous reports also showed that the secondary structural content of apoazurin and cellular retinoic acid-binding protein I was not significantly affected by the crowders [104-105]. However, in case of natively folded apo and holo-flavodoxin, and VlsE, the crowder presence in reaction medium induces the secondary structure [30-31,106].

3.5 Crowding agent counterbalances and strengthens the destabilizing action of denaturant on stability Cyt c and Mb, respectively.

Fig. 5a and Fig. 5b present the effect of temperature on visible absorption (380-600 nm) and far-UV-CD spectra (200-250 nm) of Ferrocyt *c*, respectively. Fig. 5c and Fig. 5d present the effect of temperature on visible absorption (300-600 nm) and far-UV-CD spectra (200-250 nm) of Mb, respectively. Fig. 5c also presents the effect of temperature on visible absorption (350-600 nm) spectra of Mb collected in the presence of 1.5 M GdnHCl and 5 M urea. The far-UV CD spectra of Ferrocyt *c* (Fig. 5b) and Mb (Fig. 5d) at 25 °C exhibit negative cotton effect at 222 nm that reflects the secondary structure of the native proteins. As temperature is increased from 25 to 110 °C for Ferrocyt *c* and 25 to 90 °C for Mb, the intensity of α-band (550 nm for Ferrocyt *c* (inset of Fig. 5a)) and Soret band (409 nm for Mb (Fig. 5c) and 416 nm for Ferrocyt *c* (Fig. 5a)) significantly decreases as well as the negative cotton effect at 222 nm (Figs. 5b, d) is eliminated, which reveals thermal unfolding of the heme proteins.

The UV-visible spectra of heme free Mb shows a broad spectrum between 350-400 nm [107]. The UV-visible spectra of Mb collected at 25 °C and 90 °C in the absence and presence of 1.5 M GdnHCl or 5.0 M urea suggest fallout of heme at 90 °C in the presence of 1.5 M GdnHCl or 5.0 M urea (Fig. 5c). The representative thermal denaturation curves of Ferrocyt *c* and Mb measured at different concentration of denaturant (GdnHCl or urea) in the absence and presence of 100-300 mg ml^{-1} crowder (dextran 40, dextran 70 and ficoll 70) are shown in Figs. 6a-6d and Fig. S2. Figs. 6a-6d and Fig. S2 clearly indicate that the denaturant presence shifts the thermal denaturation curves of Ferrocyt *c* and Mb to lower temperatures. However, the crowder presence opposes or potentiates such denaturant-mediated temperature shifts of Ferrocyt *c* (Figs. 6a and 6b; and Fig. S2) and Mb (Figs. 6c and 6d), respectively. The thermal unfolding curves of Ferrocyt *c* and Mb measured at different concentration of denaturant (urea or GdnHCl) in the absence and presence of 100-300 mg ml^{-1} crowder (dextran 40, dextran 70 and ficoll 70) were analyzed for thermal denaturation midpoint (T_m), enthalpy (ΔH_m) and heat capacity (ΔC_p) changes for unfolding by two-state model $N \rightleftharpoons U$ using equation (2) (material and method section)) [82, 85]. The estimated T_m, ΔH_m and ΔC_p values for Ferrocyt *c* (Tables 2-3 and Table S1) and Mb (Tables 4-5) at different concentrations of GdnHCl and urea in the absence and presence of crowding agent are summarized in Tables 2-5 and Table S1.

Fig. 7a and Fig. 7b present the effect of urea on tryptophan fluorescence emission spectra of Ferricyt *c* and Mb, respectively collected in the absence and presence of 100 mg ml^{-1} crowder (dextran 40, dextran 70 and ficoll 70) at pH 7.0, 25 °C. The data in Fig 7a and Fig. 7b suggest that the crowder presence may quench the tryptophan fluorescence of urea-denatured Ferricyt *c* and Mb. Fig. 7c and Fig. 7d show the representative tryptophan fluorescence-monitored normalized urea-induced unfolding curves of Ferricyt *c* and Mb, respectively, measured under variable concentration

of GdnHCl in the absence and presence of 100 mg ml^{-1} of crowding agent (dextran 70, dextran 40 and ficoll 70). Fig. 7c and Fig. 7d clearly indicate that the GdnHCl presence shifts the urea-induced unfolding curves of Ferricyt *c* and Mb to lower urea concentrations. However, the crowder presence opposes and potentiates such denaturant-mediated urea shifts of Ferrocyt *c* (Fig.7c) and Mb (Fig. 7d), respectively.

To determine the effects of crowding agent on denaturant-dependent denaturation free energy (ΔG_D) and surface area exposed by solvent (m_g,), the urea-induced unfolding curves of Ferricyt *c* and Mb were analyzed by assuming a two state transition between the folded (N) and unfolded (U) conformations using the procedure of Santoro and Bolen (equation (3) (material and method section)) [86]. The corresponding urea-unfolding midpoint, C_m ($=\Delta G_D/m_g$), was also calculated. The resulting values of ΔG_D, m_g and C_m are summarized in Tables 6 -7. The effect of crowding agent on the denaturant-dependent thermodynamic parameters for Ferrocyt *c* and Mb are shown in Figs. 8 &10; and Figs. 9 &10, respectively. The T_m and ΔH_m values for Ferrocyt *c* and Mb have been found to be linearly decreased with [denaturant] (Figs. 8&9 and Fig. S2). The ΔG_D and C_m values for Ferricyt *c* and Mb have been also found to be linearly decreased with GdnHCl concentration (Fig. 10). However, the crowder presence opposes and potentiates the denaturant-mediated decrease in T_m and C_m for Cyt *c* (Figs. 8&10, Fig. S2 and Tables 2-3,6) and Mb (Figs. 9&10 and Tables 4-5,7), respectively, indicating that the crowding agent presence counterbalances and strengthens the destabilizing action of denaturant on stability of Cyt *c* and Mb, respectively.

3.6 Size and shape of crowding agent modulate the effect of crowder on denaturant-dependent stability of heme proteins

A previous report showed that the size and shape of crowder can modulate the protein conformation [109]. A recent denaturant-induced equilibrium unfolding study of Ferrocyt *c* showed that the smaller sized rod shaped dextran 40 has a better stabilizing effect than the larger sized rod shaped dextran 70 and spherical shaped ficoll 70 (dextran 40 > dextran 70 > ficoll 70) [78]. However, a previous denaturant-induced equilibrium unfolding study of native apoazurin showed that the stabilizing effect of crowder is independent of the size of dextrans (dextran 20, dextran 40 and dextran 70) [104]. Thermal denaturation study of flavodoxin showed that the dextran 70 has larger stabilizing effect than the ficoll 70 [30]. These studies thus reveal that crowder of different sizes and shape exhibits distinct stabilizing effects on different proteins.

In the present case, it has been observed that denaturant decreases T_m, ΔG_D and C_m values for Cyt *c* (Figs. 8&10, Fig. S2, and Tables 2-3,6) and Mb ((Figs. 9&10, and Tables 4-5,7). However, the crowder presence counterbalances and strengthens the denaturant-mediated decreases in T_m, ΔG_D and C_m for Cyt *c* (Figs. 8&10, Fig. S2 and Tables 2-3,6) and Mb (Figs. 9&10 and Tables 4-5,7), respectively. Furthermore, the counteracting and strengthening effects of crowder on denaturant-mediated decreases in T_m, ΔG_D and C_m for Cyt *c* (Figs. 8&10, Fig. S2 and Tables 2-3,6) and Mb (Figs. 9&10 and Tables 4-5,7), respectively, typically follow the order: dextran 40 > dextran 70 > ficoll 70. This finding reveals that the size and shape of crowding agent modulate the effect of crowder on denaturant-dependent stability of heme proteins.

3.7 Presence of crowding agent stabilizes the native Cyt c but destabilizes the native Mb

In general, the influence of crowder on stability of macromolecules is expected to depend on the nature and strength of hard and soft interactions between crowder and macromolecules [110-

113]. The nonspecific chemical interactions can be attractive or repulsive. Generally, the repulsive chemical interactions contribute entropically while the attractive chemical interactions contribute enthalpically [8]. Furthermore, the repulsive chemical interactions reinforce the hard-core repulsions and cause protein stabilizing effect [8]. On the other hand, the attractive chemical interactions counteract the effect of hard-core repulsions and cause protein destabilizing effect [8]. The binding of non-inert crowders to target proteins could also occur. Earlier studies showed that the stabilizing effect of crowder on protein stability is due to purely steric excluded volume effect (*i.e.,* entropic effect) [8, 114-115]. However, some of recent reports showed that the effect of crowding agents on protein stability and folding is primarily due to enthalpic effect [12, 14, 78]. Furthermore, in some cases, the enthalpic contribution even dominates over entropic effect [12, 14, 78]. Recently, we have shown that both entropic and enthalpic effects contribute to stabilizing effect of crowder on serum transferrin stability [116].

The decrease in stability of Mb in the presence of crowder is quite different from what has been documented for proteins like ubiquitin [14], Cyt *c* [16, 71] and apoflavodoxin [31, 73] in which crowder presence increases the thermal stability of these proteins. It is inquisitive to know why crowding agent stabilizes the ubiquitin [14], Cyt *c* [16, 71] and apoflavodoxin [31, 73] but destabilizes the Mb [108, 117]? Results of previous two sections show that the crowder counterbalances and strengthens the destabilizing action of denaturant on stability of Cyt *c* and Mb, respectively. The mechanism by which a crowder counteracts the denaturant effects in Cyt *c* but potentiates the denaturant effects in Mb is not clearly understood.

An earlier work has shown that the lower m_g-values in the equilibrium unfolding curves correlate with the compaction in unfolded state [118]. Both in the absence and presence of GdnHCl, the m_g-values for Cyt *c* and Mb are lower (Tables 6-7), indicating reasonably compact unfolded

states of these proteins. If unfolded state is more compact, then it is possible that the reduced surface area may be exposed upon protein unfolding and the crowder may affect the compact unfolded state ensembles [119]. However, the m_g-values for Cyt *c* or Mb in buffer and in the presence of crowder are about similar (Tables 6-7). Tryptophan fluorescence lifetime study of Mb performed in the presence of high concentration of urea in the absence and presence of crowding agent (dextran 70 and ficoll 70) revealed that the tryptophan lifetime and hence tryptophan-heme distance was roughly same on buffer or crowding agents [108]. This finding suggests that the crowder does not provide much compaction of the denatured Mb ensemble [108]. Recent, fluorescence correlation spectroscopy (FCS) study of yeast-Cyt *c* performed with native and urea-unfolded protein in the presence of ~200 mg ml^{-1} ficoll 70 showed that the crowder significantly compacted the unfolded state due to excluded volume effect [49]. The m_g-values for yeast-Cyt *c* in buffer and in the presence of ~200 mg ml^{-1} ficoll 70 were also found about similar [49]. So, in case of Cyt *c*, regardless of unfolded-state compaction, substantial surface area may be exposed because of a rugged exterior of the conformers within the unfolded-state ensemble and the crowding presence due to steric excluded volume effect (*i.e.,* entropic effect) counterbalances the destabilizing effect of denaturant on Cyt *c* [16,71]. The current results show that due to destabilization of tertiary structure and weakening of interactions between heme and globin (Fig. S4) resulting from chemical interactions between Mb and crowders (i.e., soft interactions) (Fig. 11), the unfolded compact state of Mb does not experience the excluded volume of the crowder as other proteins like, ubiquitin [14], cyt *c* [16, 71] and apoflavodoxin [31, 73] experiences. Analysis of the effect of ficoll 70 on Trp fluorescence (Fig. S4a,b), aromatic bands at 282 and 289 nm (near-UV CD) (Fig. S4c,d), and Soret peak at 409 nm (visible absorption) (Fig. S4e,f), suggests that the crowder presence does not greatly affect the tertiary structure (Fig. S4a,c) and interactions between

heme and globin of Cyt *c* (Fig. S4e) but destabilize the tertiary structure (Fig. S4b,d) and weaken the interactions between heme and globin (Fig. S4f) of Mb.

To account whether in addition to hard-core repulsions and exclude-volume effects, the chemical interactions between crowder and protein also play important role for the observed crowder effects, the effects of crowding agents were analyzed using $T\Delta\Delta S$ *vs* $\Delta\Delta H$ plots on thermodynamics of folding of Cyt *c* and Mb. According to Daniel Harries formalism, the entropy-enthalpy plots can be used to estimate the entropic and enthalpic contributions of crowding on stability and folding of proteins [120-122]. Here, the diagonal $T\Delta\Delta S = -\Delta\Delta H$ divides the entropy-enthalpy plots into four sectors. Sector 1 and sector 2 stand for stabilizing co-solutes, while sector 3 and sector 4 stand for destabilizing co-solutes. Furthermore, the sectors 1 and 3 describe the enthalpically dominated effect, while sectors 2 and 4 describe the entropically dominated effect [120].

Fig. 10a and Fig. 10b describe the $T\Delta\Delta S$ *vs* $\Delta\Delta H$ plots for Cyt *c* and Mb in the absence and presence of denaturant (1.0 M GdnHCl or 4.5 M urea), respectively for three different crowding agents (ficoll 70, dextran 70 and dextran 40). According to Daniel Harries formalism, the $T\Delta\Delta S$ *vs* $\Delta\Delta H$ plots in Fig. 10a and Fig. 10b represent the thermodynamics of folding rather than unfolding [120-122]. Both in the absence and presence of denaturants, the data points for Cyt *c* in presence of crowder lie slightly above the upward sloping diagonal in sector 1 (Fig. 10a), which suggests that in addition to excluded volume effect (*i.e.*, entropic effect), the enthalpic effect also contributes to observed effect of crowder on stability and folding of Cyt *c*. On the other hands, both in the absence and presence of denaturants, the data points for Mb in the presence of crowder lie slightly below the upward sloping diagonal in sector 3, indicative of enthalpic dominant destabilization. Thus, the differential effect of crowding on stability of Cyt *c* and Mb suggest that hard-core repulsions,

exclude-volume effects as well as chemical interactions between crowder and protein may play important role for the observed effects. It is possible that crowding agents may interact preferentially with the unfolded state of Mb and, therefore, additionally destabilize Mb. A recent ITC and docking study revealed ficoll 70 binding to the heme moiety of native Mb [117].

4. Conclusions

Analysis of kinetic and thermodynamic parameters measured for CO dissociation reaction of NCO and MbCO under various concentrations of denaturant (GdnHCl or urea) in the absence and presence of 50-300 mg ml^{-1} of crowder (dextran 70, dextran 40, and ficoll 70) reveals that (i) crowder presence restricts the dynamics of NCO and MbCO, (ii) subdenaturing concentrations of denaturant constrain the dynamics of NCO and MbCO and inclusion of crowder further potentiates the denaturant-mediated constrained dynamics of NCO and MbCO, (iii) at relatively higher concentrations, the chaotropic action of the denaturant dominates and that unfolds the protein, (iv) within the denaturing region, the inclusion of crowding agent opposes the structural fluctuation that unfolds the protein, and (v) size and shape of crowding agent modulate the effect of crowder on denaturant-mediated restricted dynamics and structural fluctuation that unfolds the proteins. Thermodynamic analysis of thermal and urea-induced unfolding curves of Cyt *c* and Mb measured at varying concentrations of GdnHCl in the absence or presence of 100-300 mg ml^{-1} of crowder (dextran 70, dextran 40, and ficoll 70) reveals that: (i) crowder presence stabilizes the native Cyt but destabilizes the native Mb (ii) crowder presence counterbalances and potentiates the destabilizing effect of denaturants on stability of Cyt c and Mb, respectively, (iii) size and shape of crowding control the effect of crowder on denaturant-dependent stability of heme proteins, (iv) both entropic

and enthalpic effect may contribute to stabilizing effect of crowder on folding and stability of Cyt *c*, and (v) enthalpic effect (soft interactions between Mb and crowder) may contribute to destabilizing effect of crowder on stability of Mb.

Acknowledgements:

This work was supported by DST-SERB grant (EMR/2014/000242), ICMR grant (F.No. 52/6/2013-BMS) and DBT grant (BT/PR11684/BRB/10/1300/2014), Government of India.

Author Contributions: R.K. conceived the ideas. R.K., D.S.,V.K., and R.K. designed the research. R.K. (Ph.D. student) performed the research. R.K., D.S., V.K. and R.K analyzed the data. R.K., V.K. and D.S. and R.K. wrote the paper.

ASSOCIATED CONTENT

Supporting Information. Figure S1 shows CO dissociation kinetics of NCO. Tables S1 and Figure S2 show effects of crowding agents on the denaturant dependent thermal denaturation midpoint (T_m), enthalpy change (ΔH_m) and heat capacity change (ΔC_p) of Ferrocyt *c* based on absorbance at 416 nm. Figure S3 presents the far-UV CD spectra of N-state, NCO-state and UCO-state at pH, 7.0 25 °C. Figure S4 present the effect of ficoll 70 on Trp fluorescence, aromatic bands at 282 and 289 nm (near-UV CD), and Soret peak at 409 nm (visible absorption).

References:

[1] A.B. Fulton, How crowded is the cytoplasm? Cell, 30 (1982) pp. 345–347.

[2] D.S. Goodsell, Inside a living cell, Trends Biochem. Sci., 16 (1991) pp. 203–220.

[3] M.S. Cheung, D. Klimov, D. Thirumalai, Molecular crowding enhances native state stability and refolding rates of globular proteins**,** Proc. Nat. Acad. Sci. USA, 13 (2005) pp. 4753–4758.

[4] S.B. Zimmerman, S.O. Trach, Estimation of macromolecule concentrations and excluded volume effects for the cytoplasm of *Escherichia coli*, J. Mol. Biol., 222 (1991) pp. 599−620.

[5] G. Rivas, F. Ferrone, J. Herzfeld, Life in a crowded world, EMBO Rep., 5 (2004) pp. 23−27.

[6] R. J. Ellis, A. P. Minton, Cell biology: join the crowd, Nature, 425 (2003) pp. 27−28.

[7] A. P. Minton, Excluded volume as a determinant of macromolecular structure and reactivity, Biopolymers, 20 (1981) pp. 2093−2120.

[8] Y. Wang, M. Sarkar, A.E. Smith, A.S. Krois, G.J. Pielak, Macromolecular crowding and protein stability**,** J. Am. Chem. Soc., 134 (2012) pp. 16614−16618.

[9] S. B. Zimmerman, A.P. Minton, Macromolecular crowding: biochemical, biophysical, and physiological consequences, Annu. Rev. Biophys. Biomol. Struct., 22 (1993) pp. 27–65.

[10] A. P. Minton, How can biochemical reactions within cells differ from those in test tubes? J. Cell Sci., 119 (2006) pp. 2863–2869.

[11] R. J. Ellis, Macromolecular crowding: obvious but underappreciated**,** TIBS, 26 (2001) pp. 597–604.

[12] L. A. Benton, A.E. Smith, G.B. Young, G.J. Pielak, Unexpected effects of macromolecular crowding on protein stability**,** Biochemistry, 51 (2012) pp. 9773−9775.

[13] S. N. Timasheff, The control of protein stability and association by weak interactions with water: how do solvents affect these processes? Annu. Rev. Biophys. Biomol. Struct., 22 (1993) pp. 67−97.

[14] M. Senske, L. Tork, B. Born, M. Havenith, C. Herrmann, S. Ebbinghaus, Protein stabilization by macromolecular crowding through enthalpy rather than entropy**,** J. Am. Chem. Soc., 136 (2014) pp. 9036−9041.

[15] G. I. Makhatadze, P. L. Privalov, Protein interactions with urea and guanidinium chloride. A calorimetric study**,** J. Mol. Biol., 226 (1992) pp. 491−505.

[16] K. Sasahara, P. McPhie, A. P. Minton, Effect of dextran on protein stability and conformation attributed to macromolecular crowding**,** J. Mol. Biol., 326 (2003) pp. 1227–123

[17] A. Dhar, A. Samiotakis, S. Ebbinghaus, L. Nienhaus, D. Homouz, M. Gruebele, M.S. Cheung, Structure, function, and folding of phosphoglycerate kinase are strongly perturbed by macromolecular crowding, Proc. Natl. Acad. Sci. USA, 107 (2010) pp. 17586-17591.

[18] K. Aoki, M. Yamada, K. Kunida, S. Yasuda, M. Matsuda, Processive phosphorylation of ERK MAP kinase in mammalian cells**,** Proc. Natl. Acad. Sci. USA, 108 (2011) pp. 12675–12680.

[19] Y. Wang, C. Li, G. J. Pielak, Effects of proteins on protein diffusion**,** J. Am. Chem. Soc., 132 (2010) pp. 9392–9397.

[20] S.R. McGuffee, A. H. Elcock, Diffusion, crowding and protein stability in a dynamic molecular model of the bacterial cytoplasm**,** PLoS Comput. Biol., 6 (2010) pp. e1000694.

[21] C. Leduc, K. Padberg-Gehle, V. Varga, D. Helbing, S. Diez, J. Howard, Molecular crowding creates traffic jams of kinesin motors on microtubules**,** Proc. Natl. Acad. Sci. USA, 109 (2012) pp. 6100–6105.

[22] J. Batra, K. Xu, S. Qin, H. X. Zhou, Effect of macromolecular crowding on protein binding stability: modest stabilization and significant biological consequences, Biophys. J., 97 (2009) pp. 906–911.

[23] L. Huang, R. Jin, J. Li, K. Luo, T. Huang, D. Wu, W. Wang, R. Chen, G. Xiao, Macromolecular crowding converts the human recombinant PrPC to the soluble neurotoxic beta-oligomers**,** FASEB J., 24 (2010) pp. 3536–3543.

[24] Z. Zhou, X. Yan, K. Pan, J. Chen, Z. S. Xie, G. F. Xiao, F. Q. Yang, Y. Liang, Fibril formation of the rabbit/human/bovine prion proteins**,** Biophys. J., 101 (2011) pp. 1483–1492.

[25] B.V. Berg, R. J. Ellis, C.M. Dobson, Effects of macromolecular crowding on protein folding and aggregation, EMBO J., 18 (1999) pp. 6927–6933.

[26] K. X. X. Yong, T. J. Shakespeare, D. Cash, S. M. D. Henley, J. M. Nicholas, G. R. Ridgway, H. L. Golden, E. K. Warrington, A. M. Carton, D. Kaski, J. M. Schott, J. D. Warren, S. J. Crutch, Prominent effects and neural correlates of visual crowding in a neurodegenerative disease population, Brain, 137 (2014) pp. 3284–3299.

[27] E. Rivera, J. Straub, D. Thirumalai, Sequence and crowding effects in the aggregation of a 10-residue fragment derived from islet amyloid polypeptide, Biophys. J., 96 (2009) pp. 4552–4560.

[28] E. E. Wanker, Protein aggregation in Huntington's and Parkinson's disease: implications for therapy**,** Mol. Med. Today, 6 (2000) pp. 387–391.

[29] Q. Ma, J. Hu, J. Chen, Y. Liang, The role of crowded physiological environments in prion and prion-like protein aggregation, Int. J. Mol. Sci., 14 (2013) pp. 21414–21427.

[30] M. Perham, L. Stagg, P. Wittung-Stafshede, Macromolecular crowding increases structural content of folded proteins, FEBS Letters, 581 (2007) pp. 5065–5069.

[31] L. Stagg, S. Zhang, M. S. Cheung, P. Wittung-Stafshede, Molecular crowding enhances native structure and stability of alpha/beta protein flavodoxin**,** Proc. Nat. Acad. Sci. USA, 48 (2007) pp. 18976–18981.

[32] A. Kudlay, M. S. Cheung, D. Thirumalai, Crowding effects on the structural transitions in a flexible helical homopolymer, Phys. Rev. Lett., 102 (2009) pp. 118101-118104.

[33] A. P. Minton, Models for excluded volume interaction between an unfolded protein and rigid macromolecular cosolutes: macromolecular crowding and protein stability revisited, Biophys. J., 88 (2005) pp. 971−985.

[34] A. P. Minton, Effect of a concentrated "inert" macromolecular cosolute on the stability of a globular protein with respect to denaturation by heat and by chaotropes: a statistical-thermodynamic model, Biophys. J., 78 (2000) pp. 101−109.

[35] A. P. Minton, Molecular crowding: analysis of effects of high concentrations of inert cosolutes on biochemical equilibria and rates in terms of volume exclusion, Methods Enzymol., 295 (1998) pp. 127−149.

[36] J. Ådén, P. Wittung-Stafshede, Folding of an unfolded protein by macromolecular crowding in vitro, Biochemistry, 53 (2014) pp. 2271−2277.

[37] M. Erlkamp, S. Grobelny, R. Winter, Crowding effects on the temperature and pressure dependent structure, stability and folding kinetics of Staphylococcal Nuclease, Phys. Chem. Chem. Phys., 16 (2014) pp. 5965–5976.

[38] J. Bai, M. Liu, G. J. Pielak, C. Li, Macromolecular and small molecular crowding have similar effects on α-synuclein structure, Chemphyschem, 18 (2017) pp. 55–58.

[39] Y. Zhai, R. Winter, Effect of molecular crowding on the temperature-pressure stability diagram of ribonuclease A, ChemPhysChem, 14 (2013) pp. 386–393.

[40] M. Gao, R. Winter, The effects of lipid membranes, crowding and osmolytes on the aggregation and fibrillation propensity of human IAPP, *J.* Diabetes Res., (2015) pp. 849017.

[41] M. Erlkamp, J. Marion, N. Martinez, C. Czeslik, J. Peters, R. Winter, Influence of pressure and crowding on the sub-nanosecond dynamics of globular proteins, J. Phys. Chem. B, 119 (2015) pp. 4842–4848.

[42] H. Kang, P. A. Pincus, C. Hyeon, D. Thirumalai, Effects of macromolecular crowding on the collapse of biopolymers, Phys. Rev. Lett., 114 (2015) pp. 068303.

[43] F. Bergasa-Caceres, H. A. Rabitz, Macromolecular crowding facilitates the conformational transition of molten globule states of the prion protein, J. Phys. Chem. B, 120 (2016) 11093–11101.

[44] J. Groen, et al., Associative interactions in crowded solutions of biopolymers counteracts depletion effects, J. Am. Chem. Soc., 137 (2015) pp. 13041–13048.

[45] S. Patra, N. Erwin, R. Winter, Translational dynamics of lipidated ras proteins in the presence of crowding agents and compatible osmolytes, Chemphyschem, 17 (2016) pp. 2164–2169.

[46] C. Rosin, P. H. Schummel, R. Winter, Cosolvent and crowding effects on the polymerization kinetics of actin, Phys. Chem. Chem. Phys., 17 (2015) pp. 8330–8337.

[47] M. Gao, R. Winter, Kinetic insights into the elongation reaction of actin filaments as a function of temperature, pressure, and macromolecular crowding, Chemphyschem, 16 (2015) pp. 3681–3686.

[48] P. H. Schummel, M. Gao, R. Winter, Modulation of the polymerization kinetics of α/β-tubulin by osmolytes and macromolecular crowding, Chemphyschem, 18 (2017) pp. 189–197.

[49] S. S. Paul, P. Sil, R. Chakraborty, S. Haldar, K. Chattopadhyay, Molecular crowding affects the conformational fluctuations, peroxidase activity, and folding landscape of yeast cytochrome *c*, Biochemistry 55 (2016) pp. 2332–2343.

[50] G. S. Sharma, S. Mittal, L. R. Singh, Effect of Dextran 70 on the thermodynamic and structural properties of proteins, Int. J. Biol. Macromol., 79 (2015) pp. 86–94.

[51] S. Mittal, L. R. Singh, Denatured state structural property determines protein stabilization by macromolecular crowding: a thermodynamic and structural approach, PLoS One, 8 (2013) pp. e78936.

[52] J. Aden, P. Wittung-Stafshede, Folding of an unfolded protein by macromolecular crowding in vitro, Biochemistry, 53 (2014) pp. 2271–2277.

[53] K. A. Sharp, Analysis of the size dependence of macromolecular crowding shows that smaller is better, Proc. Nat. Acad. Sci. USA, 112 (2015) pp. 7990–7995.

[54] O. V. Stepananko, D. O. Roginskii, O. V. Stepanenko, I. M. Kuznetsova, V. N. Uversky, K. K. Turoverov, Structure and stability of recombinant bovine odorant-binding protein: III. Peculiarities of the wild type bOBP unfolding in crowded milieu, Peer J., 4 (2016) pp. e1642.

[55] J. C. Halpin, B. Huang, M. Sun, T.O. Street, Crowding activates heat shock protein 90, J. Biol. Chem., 291 (2016) pp. 6447–6455.

[56] S. Biswas, P. K. Chowdhury, Unusual domain movement in a multidomain protein in the presence of macromolecular crowders, Phys. Chem. Chem. Phys., 17 (2015) pp. 19820–19833.

[57] C. G. Poggi, K. M. Slade, Macromolecular crowding and the steady-state kinetics of malate dehydrogenase, Biochemistry, 54 (2015) pp. 260–267.

[58] D. Gnutt, M. Gao, O. Brylski, M. Heyden, S. Ebbinghaus, Excluded-Volume effects in living cells, Angew. Chem. Int. Ed., 54 (2015) pp. 2548–2551.

[59] I. Kuznetsova, B. Zaslavsky, L. Breydo, K. Turoverov, V. Uversky, Beyond the excluded volume effects: mechanistic complexity of the crowded milieu, Molecules, 20 (2015) pp. 1377–1409.

[60] G. B. Ralston, Effects of "crowding" in protein solutions**,** J. Chem. Edu., 67 (2005) pp. 857–860.

[61] S. B. Zimmerman, S.O. Trach, Macromolecular crowding extends the range of conditions under which DNA polymerase is functional, Biochim. Biophys. Acta, 949 (1988) pp. 297–304.

[62] P. E. Lavery, S. C. Kowalczykowski, Enhancement of recA protein-promoted DNA strand exchange activity by volume-occupying agents, J. Biol. Chem., 267 (1992) pp. 9307–9314.

[63] B. R. Somalinga, R. P. Roy, Volume exclusion effect as a driving force for reverse proteolysis. Implications for polypeptide assemblage in a macromolecular crowded milieu**,** J. Biol. Chem., 277 (2002) pp. 43253–43261.

[64] J. M. Liao, Z. Y. Mo, L. J. Wu, J. Chen, Y. Liang, Binding of calcium ions to Ras promotes Ras guanine nucleotide exchange under emulated physiological conditions, Biochim. Biophys. Acta, 1784 (2008) pp. 1560–1569.

[65] I. Pozdnyakova, P. Wittung-Stafshede, Non-linear effects of macromolecular crowding on enzymatic activity of multi-copper oxidase, Biochim. Biophys. Acta, 1804 (2010) pp. 740–744.

[66] I. Pastor, E. Vilaseca, S. Madurga, J. L. Garces, M. Cascante, F. Mas, Effect of crowding by dextrans on the hydrolysis of N-Succinyl-L-phenyl-Ala-p-nitroanilide catalyzed by α-chymotrypsin, J. Phys. Chem. B, 115 (2011) pp. 1115–1121.

[67] M. K. Suthar, P. K. Doharey, A. Verma, J. K. Saxena, Behavior of Plasmodium falciparum purine nucleoside phosphorylase in macromolecular crowded environment, Int. J. Biol. Macromol., 62 (2013) pp. 657–662.

[68] M. Jiang, Z. Guo, Effects of macromolecular crowding on the intrinsic catalytic efficiency and structure of enterobactin-specific isochorismate synthase**,** J. Am. Chem. Soc., 129 (2007) pp. 730–731.

[69] S. R. Akabayov, B. Akabayov, C. C. Richardson, G. Wagner, Molecular crowding enhanced ATPase activity of the RNA helicase eIF4A correlates with compaction of its quaternary structure and association with eIF4G, J. Am. Chem. Soc., 135 (2013) pp. 10040–10047.

[70] K. Aoki, K. Takahashi, K. Kaizu, M. Matsuda, A quantitative model of ERK MAP kinase phosphorylation in crowded media, Sci. Rep., 3 (2013) pp. 1541.

[71] A. Christiansen, Q. Wang, A. Samiotakis, M. S. Cheung, P. Wittung-Stafshede, Factors defining effects of macromolecular crowding on protein stability: an in vitro/in silico case study using cytochrome *c***,** Biochemistry, 49 (2010) pp. 6519−6530.

[72] M. M. Waegele, F. Gai, Power-law dependence of the melting temperature of ubiquitin on the volume fraction of macromolecular crowders, J. Chem. Phys., 134 (2011) pp. 095104.

[73] L. Stagg, A. Christiansen, P. Wittung-Stafshede, Macromolecular crowding tunes folding landscape of parallel α/β protein, apoflavodoxin, J. Am. Chem. Soc., 133 (2011) pp. 646−648.

[74] E. Chen, A. Christiansen, Q. Wang, M. S. Cheung, D.S. Kliger, P. Wittung-Stafshede, Effects of macromolecular crowding on burst phase kinetics of cytochrome *c* folding**,** Biochemistry, 51 (2012) pp. 9836−9845.

[75] M. Karplus, J. A. McCammon, Dynamics of proteins: elements and function, Ann. Rev. Biochem., 53 (1983) pp. 263−300.

[76] I. Bahar, T. R. Lezon, L.W. Yang, E. Eyal, Global dynamics of proteins: bridging between structure and function, Annu. Rev. Biophys., 39 (2010) pp. 23–42.

[77] H. Neuweiler, M. Lollmann, S. Doose, M. Sauer, Dynamics of unfolded polypeptide chains in

crowded environment studied by fluorescence correlation spectroscopy, J. Mol. Biol., 365 (2007) pp. 856−869.

[78] R. Kumar, D. Sharma, R. Jain, S. Kumar, R. Kumar, Role of macromolecular crowding and salt ions on the structural-fluctuation of a highly compact configuration of carbonmonoxycytochrome *c*, Biophys. Chem., 207 (2015) pp. 61−73.

[79] N. A. Farrow, O. Zhang, J. D. Forman-Kay, L. E. Kay, Comparison of the backbone dynamics of a folded and an unfolded SH3 domain existing in equilibrium in aqueous buffer. Biochemistry **34** (1995) pp. 868-878.

[80] M. Akke, J. Liu, J. Cavanagh, H. P. Erickson, A. G. Palmer, Pervasive conformational fluctuations on microsecond time scales in a fibronectin type III domain. Nat. Struct. Biol. 5 (1998) pp. 55-59.

[81] F. Natali, F. Boffi, A. Bonincontro, E. Bultrini, G. Caracciolo, S. Cinelli, G. Onori, D. Pozzi, A. C. Castellano, Changes in protein dynamics induced under Gdn–HCl denaturation Appl. Phys. A 74 (2002) S1579-S1581.

[82] R. Kumar, A.K. Bhuyan, Entropic stabilization of myoglobin in the subdenaturing concentration of guanidine hydrochloride, J. Biol. Inorg. Chem., 14 (2009) pp. 11–21.

[83] S. Mukherjee, M. M. Waegele, P. Chowdhury, L. Guo, F. Gai, Effect of macromolecular crowding on protein folding dynamics at the secondary structure level, J. Mol. Biol., 393 (2009) pp. 227−236.

[84] R. Kumar, N. P. Prabhu, M. Yadaiah, A. K. Bhuyan, Protein stiffening and entropic stabilization in the subdenaturing limit of guanidine hydrochloride**,** Biophys. J., 87 (2004) pp. 2656−2662.

[85] R. Kumar, N.P. Prabhu, D.K. Rao, A.K. Bhuyan, The alkali molten globule state of horse ferricytochrome c: Observation of cold denaturation, J. Mol. Biol., l364 (2006) pp. 483–495.

[86] M. M. Santoro, D. W. Bolen, Unfolding free energy changes determined by the linear extrapolation method. 1. Unfolding of phenylmethanesulfonyl alpha-chymotrypsin using different denaturants, Biochemistry, 27 (1988) pp. 8063−8068.

[87] M. T. Jr. Record, E. S. Courtenay, S. Cayley, H. J. Guttman, Biophysical compensation mechanisms buffering *E. coli* protein-nucleic acid interactions against changing environments**,** Trends Biochem. Sci., 23 (1998) pp. 190–194.

[88] S. Cayley, B. A. Lewis, H. J. Guttman, M. T. Record, Characterization of the cytoplasm of *Escherichia coli* K-12 as a function of external osmolarity. Implications for protein-DNA interactions in vivo, J. Mol. Biol., 222 (1991) pp. 281–300.

[89] D. Hall, A. P. Minton, Macromolecular crowding: qualitative and semiquantitative successes, quantitative challenges**,** Biochim. Biophys. Acta, 1649 (2003) pp. 127−139.

[90] J. Shin, A.G. Cherstvya, R. Metzler, Kinetics of polymer looping with macromolecular crowding: effects of volume fraction and crowder size**,** Soft Matter, 11 (2015) pp. 472–488.

[91] R. Jain, D. Sharma, R. Kumar, Effects of alcohols on the stability and low-frequency local motions that control the slow changes in structural dynamics of ferrocytochrome *c*, J. Biochem., 154 (2013) pp. 341–354.

[92] A.K. Bhuyan, Protein stabilization by urea and guanidine hydrochloride, Biochemistry, 41 (2002) pp. 13386–13394.

[93] A. M. Berghuis, G. D. Brayer, Oxidation state-dependent conformational changes in 735 cytochrome c, J. Mol. Biol., 223 (1992) pp. 959–976.

[94] J. D. Morgan, J. A. McCammon, Molecular dynamics of ferrocytochrome c: time dependence of the atomic displacements, Biopolymers, 22 (1983) pp. 1579–1593.

[95] G. I. Makhatadze, Thermodynamics of Protein Interactions with Urea and Guanidinium Hydrochloride, J. Phys. Chem. B, 103 (1999) pp. 4781–4785

[96] Y. Hagihara, S. Aimoto, A. L. Fink, Y. Goto, Guanidine hydrochloride-induced folding of proteins, J. Mol. Biol., 231 (1993) pp. 180–184.

[97] M. Yao, D. W. Bolen, How valid are denaturant-induced unfolding free energy measurements? Level of conformance to common assumptions over an extended range of ribonuclease A stability, Biochemistry, 34 (1995) pp. 3771–3781

[98] L. M. Mayr, F. X. Schmid, Stabilization of a protein by guanidinium chloride, Biochemistry, 32 (1993) pp. 7994–7998

[99] G. I. Makhatadze, M. M. Lopez, J. M. Richardson, S. T. Thomas, Anion binding to the ubiquitin molecule, Protein Sci., 7 (1998) pp. 689–697

[100] L. S. Hibbard, A. Tulinsky, Expression of functionality of alpha-chymotrypsin, Effects of guanidine hydrochloride and urea in the onset of denaturation. Biochemistry, 17 (1978) pp. 5460-5468.

[101] A. C. W. Pike, R. A. Acharya, structural basis for the interaction of urea with lysozyme. Protein Sci., 3 (1994) pp. 706-710.

[102] J. Dunbar, H. P. Yennawar, S. Banerjee, J. Luo, G. K. Farber, The effect of denaturants on protein structure. Protein Sci., 6 (1997) pp. 1272-1733.

[103] S. Kumar, D. Sharma, R. Kumar, Effect of urea and alkyl urea on the stability and structural fluctuation of theM80-containing Ω-loop of horse cytochrome c, Biochim. Biophys. Acta, 1844 (2014) pp. 641–655.

[104] A. Christiansen, P. Wittung-Stafshede, Quantification of excluded volume effects on the folding landscape of *Pseudomonas aeruginosa* apoazurin in vitro, Biophys. J., 105 (2013) pp. 1689–1699.

[105] J. Hong, L. M. Gierasch, Macromolecular crowding remodels the energy landscape of a protein by favoring a more compact unfolded state, J. Am. Chem. Soc., 2010 (132) pp. 10445–10452.

[106] D. Homouz, M. Perham, A. Samiotakis, M. S. Cheung, P. Wittung-Stafshede, Crowded, cell-like environment induces shape changes in aspherical protein, Proc. Natl. Acad. Sci. USA, 105 (2008) pp. 11754–11759.

[107] S. Uppal1, S. Salhotra1, N. Mukhi1, F. Zaidi, M. Seal, S. G. Dey, R. Bhat and S. Kundu1 Significantly Enhanced Heme Retention Ability of Myoglobin Engineered to Mimic the Third Covalent Linkage by Non-Axial Histidine to Heme (Vinyl) in *Synechocystis* Hemoglobin, J. Biol. Chem., 290 (2015) pp. 1979–1993.

[108] A. Malik, J. Kundu, S. K. Mukherjee, P. K. Chowdhury, Myoglobin unfolding in crowding and confinement, J. Phys. Chem. B, 116 (2012) pp. 12895−12904.

[109] H. Dong, S. Qin, H. X. Zhou, Effects of macromolecular crowding on protein conformational changes, PLOS Comput. Biol., 6 (2010) pp. e1000833.

[110] P. B. Crowley, K. Brett, J. Muldoon, NMR Spectroscopy reveals cytochrome c–poly (ethylene glycol) interactions, ChemBioChem, 9 (2008) pp. 685–688.

[111] Y. C. Kim, J. Mittal, Crowding induced entropy–enthalpy compensation in protein association equilibria, Phys. Rev. Lett., 110 (2013) pp. 208102–208105.

[112] S. K. Mukherjee, S. Gautam, S. Biswas, J. Kundu, P. K. Chowdhury, Do macromolecular crowding agents exert only an excluded volume effect? A protein salvation study, J. Phys. Chem. B, 119 (2015) pp. 14145-14156.

[113] A. P. Minton, Explicit incorporation of hard and soft protein-protein interactions into models for crowding effects in protein mixtures. 2. Effects of varying hard and soft interactions upon prototypical chemical equilibra, J. Phys. Chem. B, 121 (2017) pp. 5515–5522

[114] A. P. Minton, Quantitative assessment of the relative contributions of steric repulsion and chemical interactions to macromolecular crowding, Biopolymers, 99 (2013) pp. 239–244.

[115] H. X. Zhou, Polymer crowders and protein crowders act similarly on protein folding stability, FEBS Lett., 587 (2013) pp. 394−397.

[116] S. Kumar, D. Sharma, R. Kumar. Role of macromolecular crowding on stability and iron release kinetics of serum transferrin, J. Phys. Chem. B, 121 (2017), pp. 8669-8683.

[117] K. Nasreen, S. Ahamad, F. Ahmad, M.I. Hassan, A. Islam, Macromolecular crowding induces molten globule state in the native myoglobin at physiological pH, 106 (2018) Int. J. Biol. Macromol., pp. 130–139.

[118] M. Auton, D.W. Bolen. Application of the transfer model to understand how naturally occurring osmolytes affect protein stability. Methods Enzymol. 428 (207) pp 397–418.

[119] T. Mikaelsson, J. Adén, L. B. Johansson, P. Wittung-Stafshede . Direct observation of protein unfolded state compaction in the presence of macromolecular crowding, Biophys. J., 104 (2013) 694–704.

[120] L. Sapir, D. Harries, Is the depletion force entropic? Molecular crowding beyond steric interactions, Curr. Opin. Colloid Interface Sci. 20 (2015) pp 3–10.

[121] L. Sapir, and D. Harries, Origin of enthalpic depletion forces, J. Phys. Chem. Lett. 5 (2014) 1061-1065.

[122] S. Sukenik, L. Sapir, and D. Harries, Balance of enthalpy and entropy in depletion forces, Curr. Opin. Colloid Interface Sci. 18 (2013) 495-501.

Table 1. Effect of macromolecular crowding on denaturant-dependent $\Delta H_{diss}^{\ddagger}$, $\Delta G_{diss}^{\ddagger}$, $\Delta S_{diss}^{\ddagger}$ and $-T\Delta S_{diss}^{\ddagger}$ for CO dissociation reaction of NCO at pH 7.0*.

	Without crowding agents				dextran 40 (100 mg ml^{-1})			
[GdnHCl] (M)	$\Delta G_{diss}^{a\ddagger}$	$\Delta H_{diss}^{\ddagger}$	$\Delta S_{diss}^{\ddagger}$	$-T\Delta S_{diss}^{a\ddagger}$	$\Delta G_{diss}^{a\ddagger}$	$\Delta H_{diss}^{\ddagger}$	$\Delta S_{diss}^{\ddagger}$	$-T\Delta S_{diss}^{a\ddagger}$
control	22.0	24.4	8.3	−2.5	22.1	25.4	11.0	−3.3
2.3	22.3	27.3	16.8	−5.0	22.4	29.4	23.7	−7.0
4.0	21.6	21.8	0.7	−0.2	21.8	23.2	4.6	−1.4
[Urea] (M)								
5.5	22.3	27.1	16.3	−4.8	22.4	29.1	22.4	−6.7
8.5	21.7	23.3	5.0	−1.6	21.9	23.5	5.5	−1.6
	dextran 70 (100 mg ml^{-1})				ficoll 70 (100 mg ml^{-1})			
[GdnHCl] (M)	$\Delta G_{diss}^{a\ddagger}$	$\Delta H_{diss}^{\ddagger}$	$\Delta S_{diss}^{\ddagger}$	$-T\Delta S_{diss}^{a\ddagger}$	$\Delta G_{diss}^{a\ddagger}$	$\Delta H_{diss}^{\ddagger}$	$\Delta S_{diss}^{\ddagger}$	$-T\Delta S_{diss}^{a\ddagger}$
control	22.2	26.3	13.6	−4.0	22.0	24.8	10.5	−2.8
2.3	22.5	29.9	24.8	−7.4	22.4	29.0	22.2	−6.6
4.0	21.9	23.9	6.7	−2.0	21.6	22.5	2.9	−0.9
[Urea] (M)								
5.5 M	22.5	29.4	23.2	−6.9	22.3	27.8	18.6	−5.5
8.5 M	21.9	23.6	5.6	−1.7	21.8	23.4	5.3	−1.6

*$\Delta G_{diss}^{\ddagger}$, $\Delta H_{diss}^{\ddagger}$, $\Delta S_{diss}^{\ddagger}$ and $-T\Delta S_{diss}^{\ddagger}$ are reported as kcal mol^{-1}, kcal mol^{-1}, cal mol^{-1} K^{-1} and kcal mol^{-1} K^{-1}, respectively. The uncertainties associated with $\Delta G_{diss}^{\ddagger}$, $\Delta H_{diss}^{\ddagger}$, $\Delta S_{diss}^{\ddagger}$ and $-T\Delta S_{diss}^{\ddagger}$ are 0.5 kcal mol^{-1}, ±0.5 kcal mol^{-1}, 2.5 cal mol^{-1} and ±0.4 kcal mol^{-1} K^{-1}, respectively.

[a] Activation free energy ($\Delta G_{diss}^{\ddagger}$) and entropy changes ($-T\Delta S_{diss}^{\ddagger}$) are given at 25 °C.

Table 2. Effect of crowding agents on [GdnHCl]-dependent T_m, ΔH_m and ΔC_p of Ferrocyt *c* at pH 7 as monitored by visible absorbance at 550 nm*.

without crowding agents				100 mg ml^{-1} ficoll 70				100 mg ml^{-1} dextran 40			
[GdnHCl] (M)	T_m	ΔH_m	ΔC_p	[GdnHCl] (M)	T_m	ΔH_m	ΔC_p	[GdnHCl] (M)	T_m	ΔH_m	ΔC_p
0.0	373.2	115	1.5	0.0	374.2	116	1.5	0.0	375.3	122	1.5
0.25	371.6	110	1.5	0.27	372.0	114	1.5	0.27	372.3	118	1.5
0.5	367.5	106	1.5	0.53	369.6	111	1.5	0.53	369.7	113	1.5
1.0	362.3	99	1.5	1.07	364.7	104	1.5	1.07	365.8	106	1.5
1.50	356.4	92	1.5	1.60	360.0	96	1.5	1.60	361.2	101	1.5
2.30	348.8	82	1.5	2.46	353.1	88	1.5	2.46	354.7	94	1.5
2.80	346.6	79	1.5	2.99	348.4	82	1.5	2.98	350.2	86	1.5
100 mg ml^{-1} dextran 70				200 mg ml^{-1} dextran 70				300 mg ml^{-1} dextran 70			
[GdnHCl] (M)	T_m	ΔH_m	ΔC_p	[GdnHCl] (M)	T_m	ΔH_m	ΔC_p	[GdnHCl] (M)	T_m	ΔH_m	ΔC_p
0.27	373.6	117	1.5	0.29	373.5	118	1.5	0.31	-	-	-
0.53	368.3	113	1.5	0.57	370.2	113	1.5	0.62	372.8	125	1.5
1.07	366.1	105	1.5	1.15	367.6	110	1.4	1.24	366.5	118	1.4
1.60	359.5	98	1.5	1.72	364.5	105	1.4	1.86	363.5	114	1.4
2.46	353.5	90	1.5	2.64	357.4	100	1.5	2.86	359.4	110	1.5
2.98	349.6	85	1.5	3.22	352.7	91	1.5	3.48	354.9	104.0	1.5

*ΔH_m, T_m and ΔC_p are reported as kcal mol^{-1}, K, and kcal mol^{-1}K^{-1}, respectively. The uncertainties associated with ΔH_m, T_m and ΔC_p are ±1.5 kcal mol^{-1}, ±0.5 K, and ± 0.1 kcal mol^{-1}K^{-1} respectively. GdnHCl concentrations mentioned in Table 2 are corrected for crowding agents using equations (4) and (4a).

Table 3. Effect of crowding agents on [urea]-dependent ΔH_m, T_m and ΔC_p of Ferrocyt *c* (CD at 222 nm) at pH 7.0 *.

without crowding agents				200 mg ml^{-1} dextran 40				200 mg ml^{-1} dextran 70			
[Urea] (M)	T_m	ΔH_m	ΔC_p	[Urea] (M)	T_m	ΔH_m	ΔC_p	[Urea] (M)	T_m	ΔH_m	ΔC_p
0.0	371.5	115	1.4	0.0	377.1	118	1.4	0.0	372.5	116	1.4
3.0	363.4	105	1.4	3.4	370.5	115	1.4	3.4	368.1	107	1.4
4.5	358.2	98	1.5	5.2	368.5	109	1.5	5.2	364.1	103	1.4
6.5	351.1	93	1.4	7.5	360.9	104	1.5	7.5	358.6	92	1.4
8.0	345.0	80	1.4	9.2	357.8	98	1.4	9.2	355.0	88	1.5

200 mg ml^{-1} ficoll 70			
[Urea] (M)	T_m	ΔH_m	ΔC_p
0.0	370.9	117	1.4
3.4	367.1	104	1.4
5.2	361.1	99	1.4
7.5	357.1	90	1.5
9.2	351.3	84	1.4

*ΔH_m, T_m and ΔC_p are reported as kcal mol^{-1}, K, and kcal mol^{-1}K^{-1}, respectively. The uncertainties associated with ΔH_m, T_m and ΔC_p are ±1.5 kcal mol^{-1}, ±0.5 K, and ± 0.1 kcal mol^{-1}K^{-1} respectively. Urea concentrations mentioned in Table 3 are corrected for crowding agents using equations (4) and (4a).

Table 4. Effect of crowding agents on [GdnHCl]-dependent ΔH_m, T_m and ΔC_p of Mb at pH 7 as monitored by visible absorbance at 409 nm*.

without crowding agents				200 mg ml^{-1} ficoll 70				200 mg ml^{-1} dextran 40			
[GdnHCl] (M)	T_m	ΔH_m	ΔC_p	[GdnHCl] (M)	T_m	ΔH_m	ΔC_p	[GdnHC] (M)	T_m	ΔH_m	ΔC_p
0.0	355.2	110	2.4	0.0	349.4	101	2.3	0.0	352.9	107	2.3
0.1	352.7	101	2.3	0.11	346.2	92	2.3	0.11	347.2	95	2.3
0.25	348.8	98	2.3	0.29	342.4	88	2.3	0.29	345.0	90	2.4
0.5	343.0	90	2.3	0.57	338.7	80	2.3	0.57	341.8	85	2.3
0.75	338.8	81	2.3	0.86	332.0	67	2.3	0.86	335.1	73	2.3
1.0	334.5	70	2.3	1.15	328.0	60	2.4	1.15	332.2	66	2.3

200 mg ml^{-1} dextran 70			
[GdnHCl] (M)	T_m	ΔH_m	ΔC_p
0.0	352.3	103	2.3
0.11	347.2	98	2.3
0.29	343.5	89	2.3
0.57	340.8	82	2.3
0.86	333.7	72	2.4
1.15	330.7	64	2.4

*ΔH_m, T_m and ΔC_p are reported as kcal mol^{-1}, K, and kcal mol^{-1}K^{-1}, respectively. The uncertainties associated with ΔH_m, T_m and ΔC_p are ±1.5 kcal mol^{-1}, ±0.5 K, and ± 0.1 kcal mol^{-1}K^{-1} respectively. GdnHCl concentrations mentioned in Table 4 are corrected for crowding agents using equations (4) and (4a).

Table 5. Effect of crowding agents on [Urea]-dependent ΔH_m, T_m and ΔC_p of Mb (CD at 222 nm) at pH 7.0*.

without crowding agents				100 mg ml^{-1} dextran 40				100 mg ml^{-1} dextran 70			
[Urea](M)	T_m	ΔH_m	ΔC_p	[Urea] (M)	T_m	ΔH_m	ΔC_p	[Urea] (M)	T_m	ΔH_m	ΔC_p
0.0	356.0	110	2.3	0.0	353.6	105	2.3	0.0	353.0	103	2.4
1.0	353.0	103	2.4	1.07	351.9	99	2.3	1.07	349.3	94	2.3
2.0	346.8	92	2.3	2.15	345.6	90	2.3	2.15	344.5	85	2.3
3.0	341.8	82	2.3	3.22	341.0	78	2.3	3.22	341.0	75	2.3
4.5	331.7	69	2.4	4.84	329.5	66	2.3	4.84	327.7	64	2.3

100 mg ml^{-1} ficoll 70			
[Urea] (M)	T_m	ΔH_m	ΔC_p
0.0	350.1	100	2.3
1.07	346.1	92	2.3
2.15	343.5	80	2.4
3.22	337.7	70	2.3
4.84	326.5	60	2.3

*ΔH_m, T_m and ΔC_p are reported as kcal mol^{-1}, K, and kcal mol^{-1}K^{-1}, respectively. The uncertainties associated with ΔH_m, T_m and ΔC_p are ±1.5 kcal mol^{-1}, ±0.5 K, and ± 0.1 kcal mol^{-1}K^{-1} respectively. Urea concentrations mentioned in Table 5 are corrected for crowding agents using equations (4) and (4a).

Table 6. Dependence of the ΔG_D, m_g and C_m of Ferricyt *c* on [GdnHCl] in the absence and presence of 100 mg ml^{-1} crowding agents at pH 7.0 as monitored by Trp fluorescence (ex: 280; em: 365nm)*.

without crowding agents				100 mg ml^{-1} dextran 40			
[GdnHCl] (M)	C_m (M)	ΔG_D (kcal mol^{-1})	m_g (kcalmol^{-1}M^{-1})	GdnHCl (M)	C_m (M)	ΔG_D (kcal mol^{-1})	m_g (kcalmol^{-1} M^{-1})
0.0	7.6	8.6	1.1	0.0	8.6	11.8	1.4
0.25	6.3	7.9	1.2	0.27	7.4	9.5	1.3
0.5	5.6	6.9	1.2	0.53	6.5	8.0	1.2
1.0	4.3	5.7	1.3	1.06	5.3	6.9	1.3
2.0	2.0	3.1	1.5	2.12	2.8	4.7	1.7

100 mg ml^{-1} dextran 70				100 mg ml^{-1} ficoll 70			
[GdnHCl] (M)	C_m (M)	ΔG_D (kcal mol^{-1})	m_g kcalmol^{-1} M^{-1})	GdnHCl (M)	C_m (M)	ΔG_D (kcal mol^{-1})	m_g (kcalmol^{-1} M^{-1})
0.0	8.4	11.1	1.3	0.0	8.3	10.3	1.2
0.27	7.2	9.1	1.3	0.27	7.2	8.6	1.2
0.53	6.4	7.4	1.2	0.53	6.3	7.3	1.2
1.06	5.2	6.5	1.2	1.06	5.1	6.0	1.2
2.12	2.7	4.5	1.6	2.12	2.6	4.0	1.6

*The uncertainties associated with ΔG_D, m_g, and C_m are ±0.5 (kcal mol^{-1}), ±0.2 (kcal mol^{-1} M^{-1}) and ±0.2 (M), respectively. GdnHCl concentrations mentioned in Table 6 are corrected for crowding agents using equations (4) and (4a).

Table 7. Dependence of the ΔG_D, m_g and C_m of Mb on [GdnHCl] in the absence and presence of 100 mg ml^{-1} crowding agents at pH 7.0 as monitored by fluorescence (ex: 280; em: 365nm)*.

without crowding agents				100 mg ml^{-1} dextran 40			
[GdnHCl] (M)	C_m (M)	ΔG_D (kcal mol^{-1})	m_g ($kcalmol^{-1}M^{-1}$)	GdnHCl (M)	C_m (M)	ΔG_D (kcal mol^{-1})	m_g ($kcalmol^{-1}$ M^{-1})
0.0	5.6	7.3	1.3	0.0	5.3	7.0	1.3
0.25	4.5	5.7	1.3	0.27	3.8	5.1	1.3
0.5	3.5	4.0	1.2	0.53	3.2	4.0	1.2
0.75	3.1	2.6	1.1	0.8	2.3	2.4	1.1
100 mg ml^{-1} dextran 70				100 mg ml^{-1} ficoll 70			
[GdnHCl] (M)	C_m (M)	ΔG_D (kcal mol^{-1})	m_g ($kcalmol^{-1}$ M^{-1})	GdnHCl (M)	C_m (M)	ΔG_D (kcal mol^{-1})	m_g ($kcalmol^{-1}$ M^{-1})
0.0	4.8	6.7	1.4	0.0	4.7	6.5	1.4
0.27	3.7	4.8	1.3	0.27	3.5	3.5	1.0
0.53	3.1	3.0	1.0	0.53	2.9	2.5	0.9
0.8	1.9	2.2	1.1	0.8	1.8	1.7	1.0

*The uncertainties associated with ΔG_D, m_g, and C_m are ±0.8 (kcal mol^{-1}), ±0.1 (kcal mol^{-1} M^{-1}) and ±0.3 (M), respectively. GdnHCl concentrations mentioned in Table 7 are corrected for crowding agents using equations (4) and (4a).

Figure Legend

Fig.1. Effect of crowding agent on the dynamics of MbCO. Panel (a) shows the slow single-phase CO replacement from MbCO by hexacyanoferrate ion (τ =32 min., 22°C). The MbCO + CN^- → MbCN + CO reaction was probed at 421 nm in phosphate buffer at pH 7.0, 22 °C. (b) Variation of log k_{diss} with [Crowding agent] at pH 7.0, 22 °C (Ficoll 70 (□), dextran 40 (◊) and dextran 70 (◆)). The log $k_{diss}$with [Crowding agent] data in panel (b) are fitted to a mono-exponential decay function.

Fig.2. Effect of crowding agents on the denaturants-dependent dynamics of NCO and MbCO. Panel (a) presents the denaturant-dependence of log k_{diss} for NCO in the absence (GdnHCl (●), urea (○)) and presence of 50 mg ml^{-1} (urea (□)), 100 mg ml^{-1} (GdnHCl (▲), urea (Δ)) and 200 mg ml^{-1} (GdnHCl (■)) of dextran 70 at pH 7.0, 22 °C. Panel (b) presents the denaturant-dependence of log k_{diss} for NCO in the absence (GdnHCl (●), urea (○)) and presence of 50 mg ml^{-1} (urea (□)), 100 mg ml^{-1} (GdnHCl (▼), urea (▽)), and 200 mg ml^{-1} (GdnHCl (▲)) of ficoll 70 at pH 7.0, 22 °C. Panel (c) presents the denaturant-dependence of log k_{diss} for NCO in the presence of 100 mg ml^{-1} of dextran 40 (urea (◆), GdnHCl (◊)), dextran 70 (GdnHCl (■), urea (Δ)), and ficoll 70 (GdnHCl (▼), urea (▽)) at pH 7.0, 22°C. Panel (d) presents the GdnHCl-dependence of log k_{diss} for MbCO in the absence (○) and presence of 200 mg ml^{-1} of dextran 40 (◊), ficoll 70 (□) and dextran 70 (◆) at pH 7.0, 22°C. The GdnHCl and urea concentration in log k_{diss} vs [Denaturants] plots are those corrected for crowding agents using equations (4) and (4a). The solid lines are just guide the eye. All the experiments are carried out in 50 mM phosphate buffer.

Fig.3. Effect of crowding agents on denaturant-dependent activation thermodynamic parameters of CO dissociation reaction of NCO at pH 7.0. Panel (a) shows Eyring plots for the CO dissociation reaction of NCO in the absence of additive (phosphate buffer (PB) only) (○) and at 2.3 M GdnHCl (Δ), 4 M GdnHCl (●), 2.3 M GdnHCl with 100 mg ml^{-1}crowding agent (dextran 70 (□), dextran 40 (▲) and ficoll 70 (◆)) and 4 M GdnHCl with 100 mg ml^{-1}crowding agent (dextran 70 (■), dextran 40 (▼) and ficoll 70 (◊)). Panel (b) shows Eyring plots for the CO dissociation reaction of NCO in the absence of additive (PB only) (○) and at 5.5 M urea (Δ), 8.5 M urea (●)), 5.5 M urea with 100 mg ml^{-1} crowding agents (dextran 70 (■), dextran 40 (▽) and ficoll 70 (◆)) and 8.5 M urea with 100 mg ml^{-1}crowding agents (dextran 70 (□), dextran 40 (▼) and ficoll 70 (◊)). The solid lines are fitted according to Eyring equation (equation (1)) [78].

Fig.4. Effect of crowding agents on the denaturant dependent-secondary structure of Ferricyt *c* and Mb at pH 7.0. Panel (a) shows the far-UV CD spectra of Ferricyt *c* collected in the absence of crowding agents (phosphate buffer (PB only)) (solid black line) and in presence of ~ 2 .0 M urea (dotted black line), 9.0 M urea (black short line) and with 200 mg ml^{-1} of dextran 40 (2.0 M urea (blue solid line), 9.0 M urea (blue short line)), dextran 70 (2.0 M urea (green solid line), 9.0 M urea (green short line)) and ficoll 70 (2M urea (gray solid line), 9.0 M urea (gray short line)) at pH 7, 25 °C. Panel (b) shows the far-UV CD spectra of Mb collected in the absence of additives (phosphate buffer (PB)) (solid black line) and in presence of ~ 2M urea (dotted black line), 9.0 M urea (black short line) and with 200 mg ml^{-1} of dextran 40 (2.0 M urea (blue solid line), 9.0 M urea (blue short line)), dextran 70 (2M urea (green solid line), 9.0 M urea (green short line)) and ficoll 70 (2M urea (gray solid line), 9.0 M urea (gray short line)) at pH 7, 25 °C.

Fig.5. Effect of temperature on the visible absorbance and far-UV CD spectra of Ferrocyt *c* and Mb at pH 7.0. Panels (a) and (b) show the visible absorption and far-UV CD spectra of Ferrocyt *c*, respectively, collected at 25 °C (solid line) and 110 °C (dotted line), pH 7.0. The inset of panel (a) shows the effect of temperature on α-band (550 nm) of Ferrocyt *c* at pH 7.0 (25 °C (solid line) and 110 °C (dotted line)). Panels (c) and (d) show the visible absorption and far-UV CD spectra of Mb, respectively, collected at 25 ºC (solid line) and 90 ºC (dotted line), pH 7.0. Panel (c) also shows the visible absorption spectra of Mb, collected in the presence of 1.5 M GdnHCl at 25 ºC (green solid line) and 90 ºC (green dotted line), and 5.0 M urea at 25 ºC (blue solid line) and 90 ºC (blue dotted line), pH 7.0.

Fig.6. Effect of crowding agents on the denaturant-dependent thermal unfolding of Ferrocyt *c* and Mb at pH 7.0. Panel (a) represents the thermal denaturation curves of Ferrocyt *c* monitored at 550 nm as the change in absorption coefficient at 0.5 M GdnHCl (○), 0.5 M GdnHCl with 100 mg ml^{-1} dextran 40 (Δ), 0.5 M GdnHCl with 100 mg ml^{-1} dextran 70 (●), 2.3 M GdnHCl (▲), 2.3 M GdnHCl with 100 mg ml^{-1} dextran 40 (□), 2.3 M GdnHCl with 100 mg ml^{-1} ficoll 70 (★), 2.3 GdnHCl with 100 mg ml^{-1} dextran 70 (▽), 2.3 M GdnHCl with 200 mg ml^{-1} of dextran 70 (▼). (b) Normalized thermally-induced unfolding curves of Ferrocyt *c* monitored at CD-222 nm at 3 M urea (○), 8 M urea (■), 8 M urea with 200 mg ml^{-1} dextran 70 (Δ), 3 M urea with 200 mg ml^{-1} dextran 70 (●), 8 M urea with 200 mg ml^{-1} dextran 40 (▼), 3 M urea with 200 mg ml^{-1} dextran 40 (▲), 8 M urea with 200 mg ml^{-1} ficoll 70 (◊), 3 M urea with 200 mg ml^{-1} ficoll 70 (▽). Panel (c) represents the thermal denaturation curves of Mb monitored at 409 nm as change in absorption coefficient in absence of additives (●) and in the presence of 0.5 M GdnHCl (▲), 0.5 M GdnHCl with 200 mg ml^{-1} of crowding agent (dextran 40 (▲), dextran 70 (▽) and ficoll 70 (○)). (d) Normalized thermally

induced unfolding curves of Mb monitored at CD-222 nm in the presence of 1.0 M urea (○), 4.5 M urea (Δ) and 1.0 M urea with 100 mg ml^{-1} dextran 70 (▽), 4.5 M urea with 100 mg ml^{-1} dextran 70 (▼), 1.0 M urea with 100 mg ml^{-1} dextran 40 (▲), 4.5 M urea with 100 mg ml^{-1} dextran 40 (□), 1.0 M urea with 100 mg ml^{-1} ficoll 70 (●), 4.5M urea with 100 mg ml^{-1} ficoll 70 (◊), at pH 7.0. The solid curves in panels (a), (b), (c) and (d) represent nonlinear least-squares fits to equation (2)) [82, 85].

Fig.7. Effects of crowding agents on the GdnHCl-dependent urea-induced unfolding of Ferricyt *c* and Mb at pH 7.0, 25°. Panels (a) and (b) present the tryptophan fluorescence emission spectra of native Cyt c and Mb, respectively (in buffer only (long dash line), 9.0 M urea (solid line), 9.0 M urea with 100 mg ml^{-1} ficoll 70 (dash dot dot line), 9.0 M urea with 100 mg ml^{-1} dextran 70 (dotted line), and 9.0 M urea with 100 mg ml^{-1} dextran 40 (short dash line)) at pH 7 25 °C. Panel (c) show the fluorescence-monitored normalized urea-induced unfolding curves of Ferricyt *c* measured in the absence (PB only) (◆), presence of 1.0 M GdnHCl (◇) and 1.0 M GdnHCl with 100 mg ml^{-1} of dextran 70 (■), dextran 40 (○), ficoll 70 (Δ) at pH 7.0 and 25°C. Panel (d) shows the fluorescence-monitored normalized urea-induced unfolding curves of Mb in the absence (PB only) (◆) and presence of 0.5 M GdnHCl (◇) and 0.5 M GdnHCl with 100 mg ml^{-1} of dextran 70 (■), dextran 40 (○), ficoll 70 (Δ) at pH 7.0 and 25°C. The solid curves represent nonlinear least-squares fits according to the standard two-state equation (Equation (3)) [82]. In panels (c) and (d) the urea concentration are those corrected for crowding agents using equations (4) and (4a).

Fig.8. Effects of crowding agents on the denaturant-dependent T_m and ΔH_m of Ferrocyt *c* at pH 7.0. Panels (a) and (b) shows the variations in T_m and ΔH_m, respectively for Ferrocyt *c* (absorbance 550

nm) as the function of [GdnHCl] in the absence (PB only) (○) and presence of 100 mg ml^{-1} (dextran 40 (Δ), dextran70 (●), ficoll70 (∇)), 200 mg ml^{-1} of dextran 70 (▲) and 300 mg ml^{-1} of dextran 70 (■) at pH 7.0. Panels (c) and (d) shows the variations in T_m and ΔH_m, respectively for Ferrocyt *c* (CD 222 nm) as the function of [urea], in the absence (PB only) (○), and presence of 200 mg ml^{-1} crowding agent (dextran 40 (Δ), dextran70 (●) and ficoll 70 (▽)) at pH 7.0. The parameters are summarized in Table 2 (Absorbance 550 nm) and Table 3 (CD 222 nm). The solid lines in panels (a) to (d) represent linear least-squares fit of the data. The GdnHCl and urea concentration in T_m and ΔH_m, vs [Denaturants] plots are those corrected for crowding agents using equations (4) and (4a).

Fig.9. Effect of crowding agents on the denaturant-dependent T_m and ΔH_m of Mb at pH 7.0. Panels (a) and (b) show the variations in T_m and ΔH_m, respectively for Mb (absorbance 409 nm) as the function of [GdnHCl] in the absence (PB only) (○), and presence of 200 mg ml^{-1} crowding agent (dextran 40 (Δ), dextran70 (◆), ficoll70 (□)) at pH 7.0. Panels (c) and (d) show the variation in T_m and ΔH_m, respectively for Mb (CD 222 nm) as the function of [urea] in the absence (○), and presence of 100 mg ml^{-1} crowding agent (dextran 40 (Δ), dextran70 (◆), ficoll70 (□)) at pH 7.0. The parameters are summarized in Table 4 (absorbance 409 nm) and Table 5 (CD 222 nm). The solid lines in panels (a) to (d) represent linear least-squares fit of the data. The GdnHCl and urea concentration in T_m and ΔH_m, vs [Denaturants] plots are those corrected for crowding agents using equations (4) and (4a).

Fig.10. Effects of crowding agents on the GdnHCl-dependent thermodynamic stability of Ferricyt *c* and Mb at pH 7.0, 25°. Panels (a) and (b) show the GdnHCl-dependence variation of the change in

unfolding free energy, ΔG_D, for Ferricyt *c* and Mb, respectively in the absence of crowder (PB only) (◆) and in the presence of 100 mg ml^{-1} of dextran 40 (●), dextran 70 (□) and ficoll 70 (Δ) at pH 7.0 and 25°C. Panels (c) and (d) show the GdnHCl-dependence variation of the urea unfolding midpoint, C_m, of Ferricyt *c* and Mb, respectively in the absence of crowder (PB only) (◆) and in the presence of 100 mg ml^{-1} of dextran 40 (●), dextran 70 (□) and ficoll 70 (Δ) at pH 7.0 and 25 °C. The thermodynamic parameters are listed in Table 6 (Ferricyt *c*) and Table 7 (Mb). The solid lines in panel (a), (b), (c) and (d) represent linear least-squares fit of the data. The GdnHCl concentration in C_m and ΔG_D vs [Denaturants] plots in panels (a)-(d) are those corrected for crowding agents using equation (4).

Fig.11. The $T\Delta\Delta S$ and $\Delta\Delta H$ plot for thermodynamics of folding of Cyt *c* and Mb for three different crowding agents (dextran 70, dextran 40, and ficoll 70) at pH 7. Panel (a) presents the $T\Delta\Delta S$ and $\Delta\Delta H$ plots for Cyt *c* (based on absorbance at 550 nm) in the absence of denaturant (PB only (◑), 100 mg ml^{-1} dextran 40 (▼), 100 mg ml^{-1} dextran 70 (▲), 200 mg ml^{-1} dextran 70 (■), and 100 mg ml^{-1} ficoll 70 (●)). Panel (a) also presents the $T\Delta\Delta S$ and $\Delta\Delta H$ plots for Mb (based on absorbance at 409 nm and CD at 222 nm) in the absence of denaturant (PB only (◑), 100 mg ml^{-1} dextran 40 (∇), 100 mg ml^{-1} dextran 70 (Δ), 100 mg ml^{-1} ficoll 70 (○), 200 mg ml^{-1} dextran 40 (☆), 200 mg ml^{-1} dextran 70 (◊), and 200 mg ml^{-1} ficoll 70 (□)). Panel (b) presents the $T\Delta\Delta S$ and $\Delta\Delta H$ plot for Cyt *c* (based on absorbance at 550 nm and CD at 222 nm) in the presence of denaturant (1.0 M GdnHCl or 4.5 M urea (◑), 1.0 M GdnHCl with 100 mg ml^{-1} dextran 40 (▼), 1.0 M GdnHCl with 100 mg ml^{-1} dextran 70 (▲), 1.0 M GdnHCl with 100 mg ml^{-1} ficoll 70 (●), 4.5 M urea with 200 mg ml^{-1} dextran 40 (♦), 4.5 M urea with 200 mg ml^{-1} dextran 70 (★), and 4.5 M urea with 200 mg ml^{-1} ficoll 70 (■). Panel (b) also presents the $T\Delta\Delta S$ and $\Delta\Delta H$ plot for Mb (based on absorbance at 409 nm and CD at 222

nm) in the presence of denaturant (1.0 M GdnHCl or 4.5 M urea (◑), 1.0 M GdnHCl with 200 mg ml^{-1} dextran 40 (∇), 1.0 M GdnHCl with 200 mg ml^{-1} dextran 70 (Δ), 1.0 M GdnHCl with 200 mg ml^{-1} ficoll 70 (○), 4.5 M urea with 100 mg ml^{-1} dextran 40 (◊), 4.5 M urea with 100 mg ml^{-1} dextran 70 (☆), and 4.5 M urea with 100 mg ml^{-1} ficoll 70 (□).

Fig.1

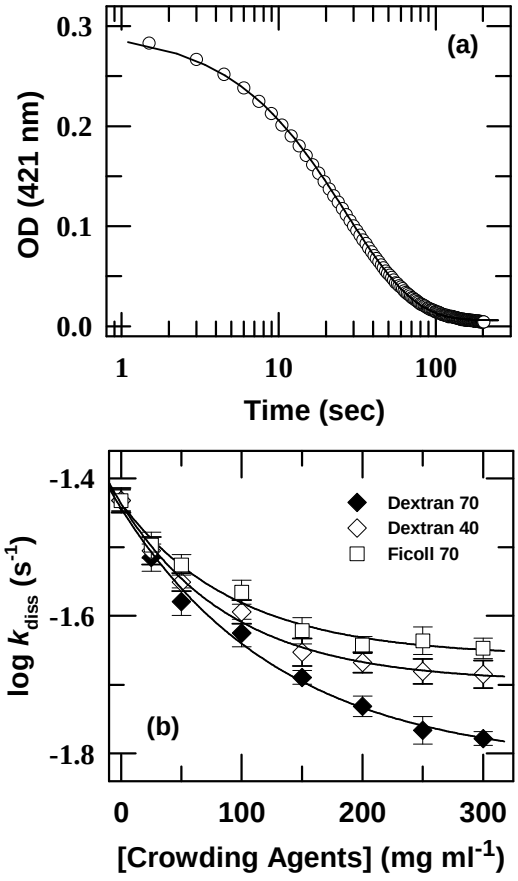
0.3
0.2
0.1
0.0
OD (421 nm)
(a)
1
10
100
Time (sec)
-1.4
-1.6
-1.8
log k_{diss} (s^{-1})
Dextran 70
Dextran 40
Ficoll 70
(b)
0
100
200
300
[Crowding Agents] (mg ml^{-1})

Fig.2

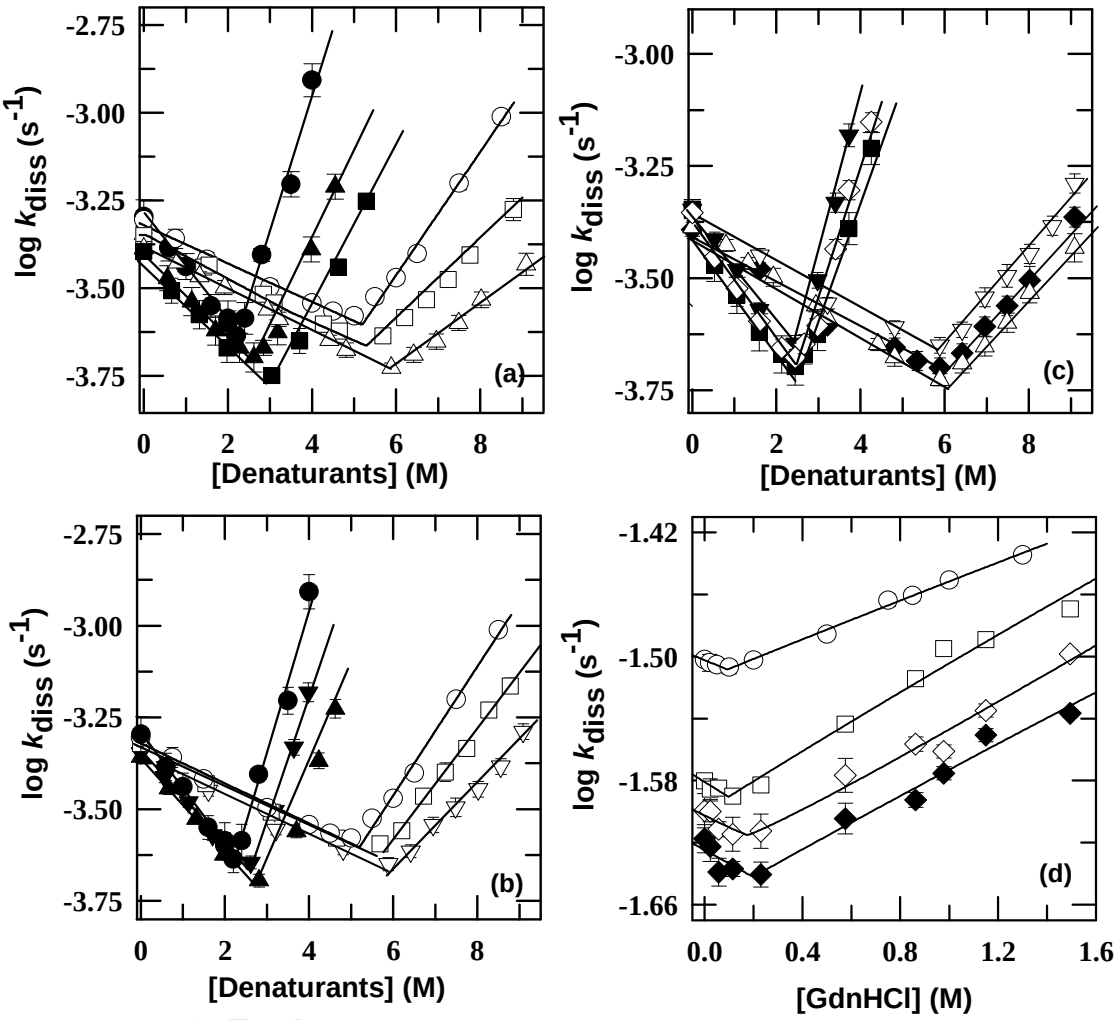
log k_{diss} (s^{-1})
-2.75
-3.00
-3.25
-3.50
-3.75
(a)
0
2
4
6
8
[Denaturants] (M)
-3.00
-3.25
-3.50
-3.75
(c)
[Denaturants] (M)
(b)
[Denaturants] (M)
-1.42
-1.50
-1.58
-1.66
(d)
0.0
0.4
0.8
1.2
1.6
[GdnHCl] (M)

Fig.3

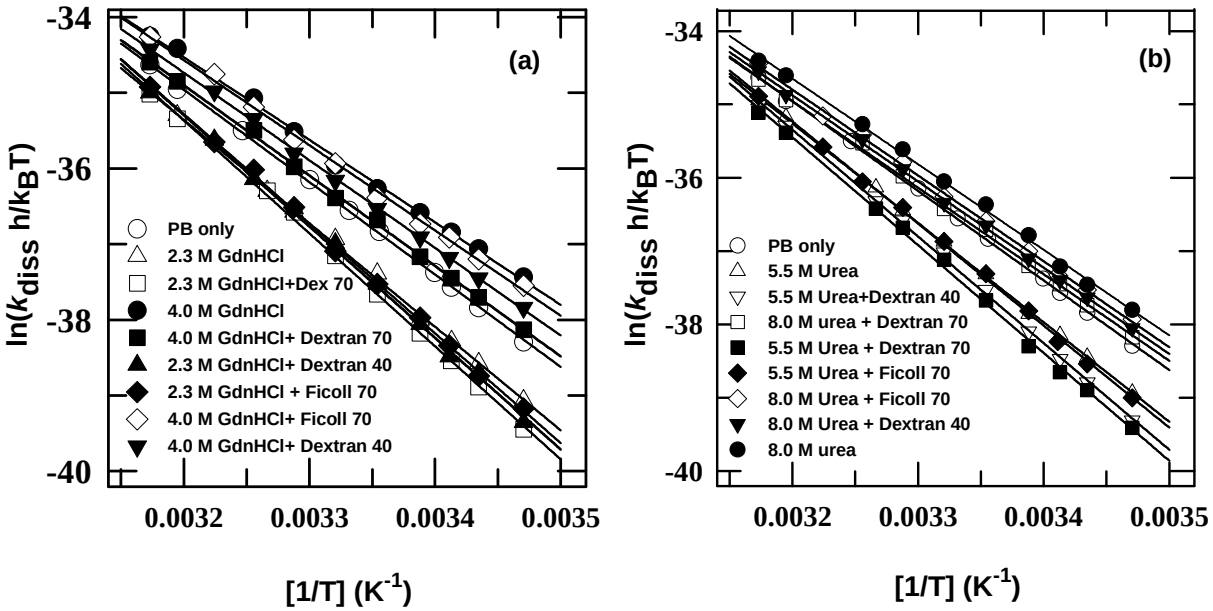

Fig.4

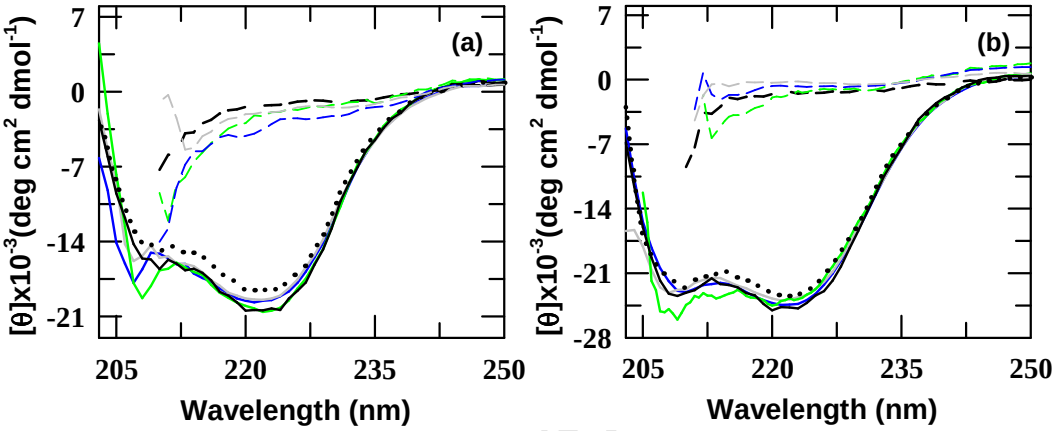

Fig. 5

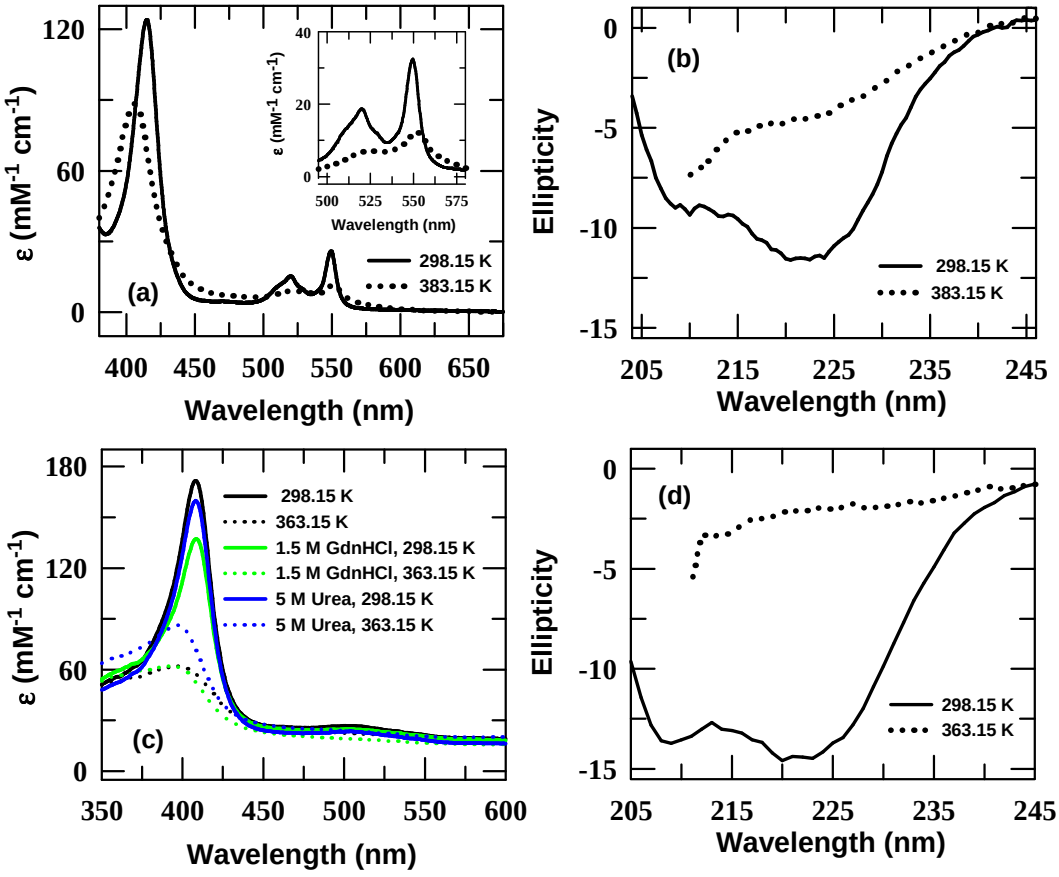
(a)
ε (mM-1 cm-1)
Wavelength (nm)
298.15 K
383.15 K
(b)
Ellipticity
Wavelength (nm)
298.15 K
383.15 K
(c)
ε (mM-1 cm-1)
Wavelength (nm)
298.15 K
363.15 K
1.5 M GdnHCl, 298.15 K
1.5 M GdnHCl, 363.15 K
5 M Urea, 298.15 K
5 M Urea, 363.15 K
(d)
Ellipticity
Wavelength (nm)
298.15 K
363.15 K

Fig. 6

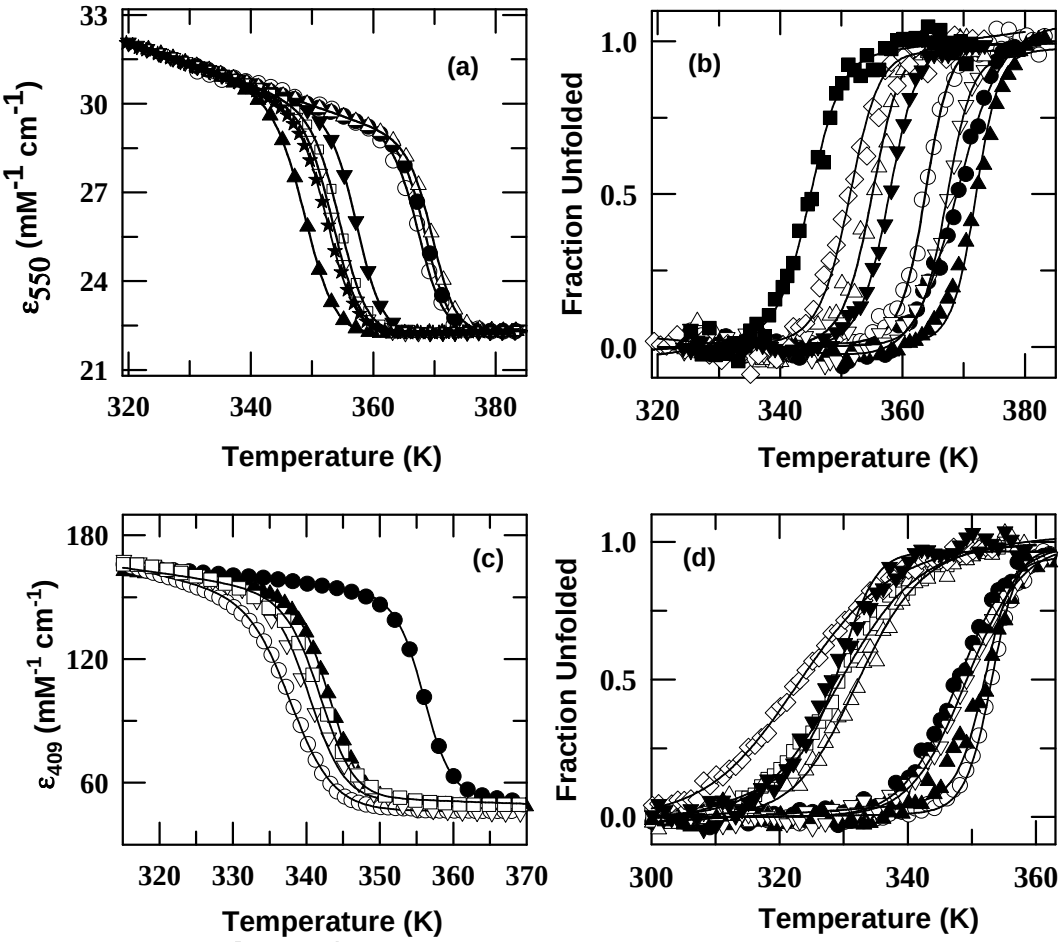
(a)
ε_{550} (mM^{-1} cm^{-1})
33
30
27
24
21
320
340
360
380
Temperature (K)
(b)
Fraction Unfolded
1.0
0.5
0.0
320
340
360
380
Temperature (K)
(c)
ε_{409} (mM^{-1} cm^{-1})
180
120
60
320
330
340
350
360
370
Temperature (K)
(d)
Fraction Unfolded
1.0
0.5
0.0
300
320
340
360
Temperature (K)

Fig. 7

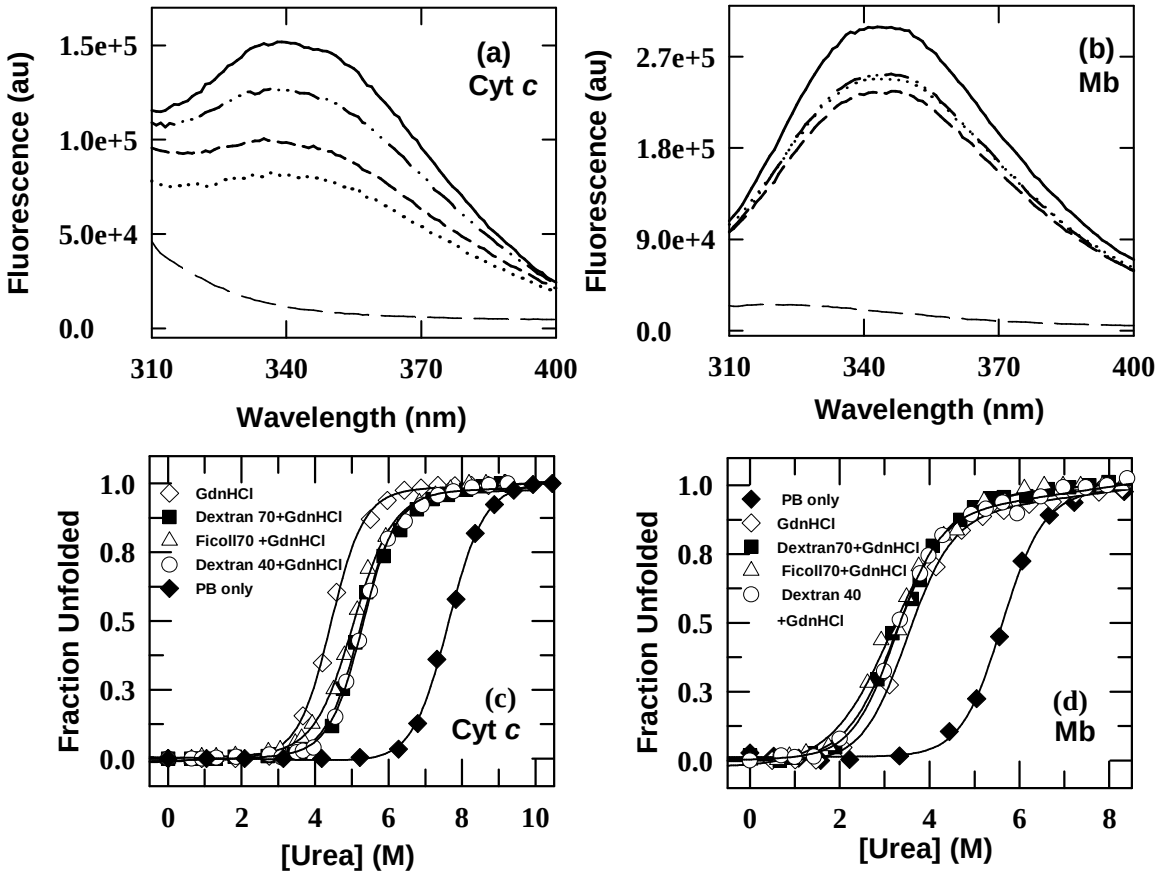
(a)
Cyt c
Fluorescence (au)
1.5e+5
1.0e+5
5.0e+4
0.0
310
340
370
400
Wavelength (nm)
(b)
Mb
Fluorescence (au)
2.7e+5
1.8e+5
9.0e+4
0.0
310
340
370
400
Wavelength (nm)
(c)
Cyt c
Fraction Unfolded
GdnHCl
Dextran 70+GdnHCl
Ficoll70 +GdnHCl
Dextran 40+GdnHCl
PB only
1.0
0.8
0.5
0.3
0.0
0
2
4
6
8
10
[Urea] (M)
(d)
Mb
Fraction Unfolded
PB only
GdnHCl
Dextran70+GdnHCl
Ficoll70+GdnHCl
Dextran 40
+GdnHCl
1.0
0.8
0.5
0.3
0.0
0
2
4
6
8
[Urea] (M)

Fig. 8

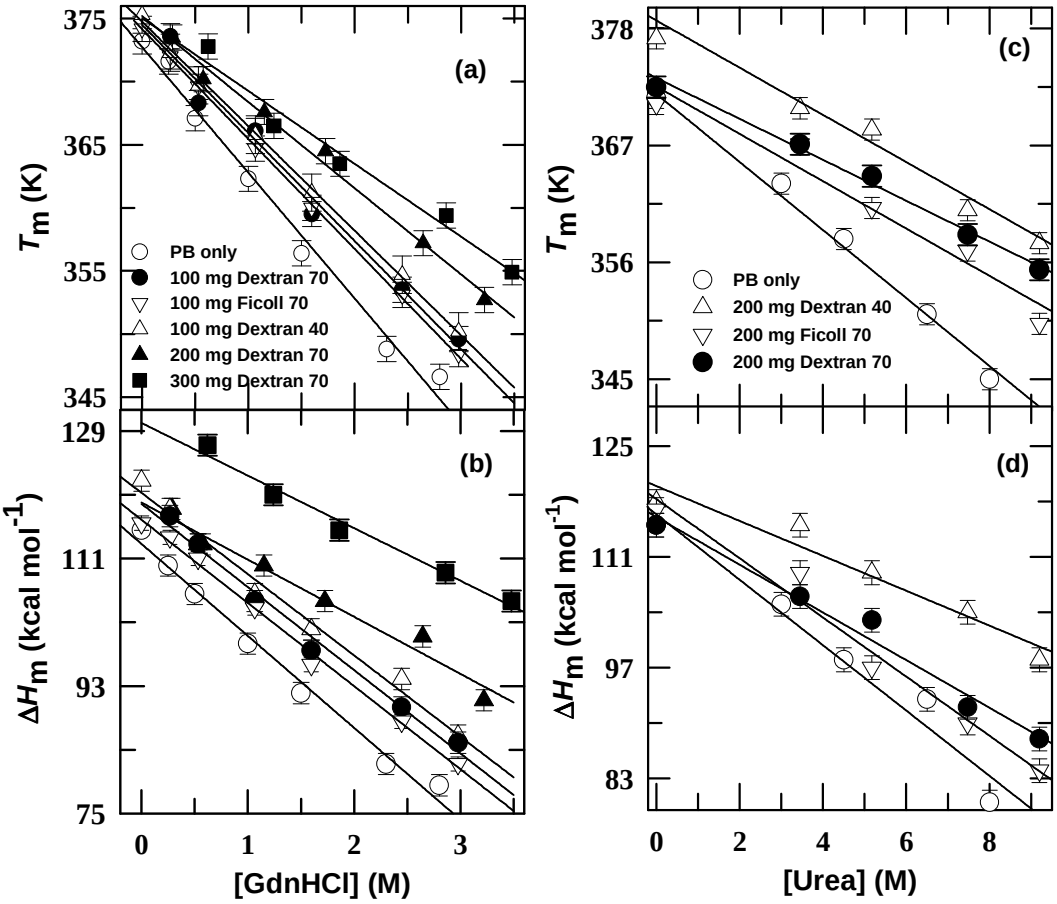
(a)
(b)
(c)
(d)
T_m (K)
ΔH_m (kcal mol^{-1})
PB only
100 mg Dextran 70
100 mg Ficoll 70
100 mg Dextran 40
200 mg Dextran 70
300 mg Dextran 70
200 mg Dextran 40
200 mg Ficoll 70
200 mg Dextran 70
[GdnHCl] (M)
[Urea] (M)

Fig. 9

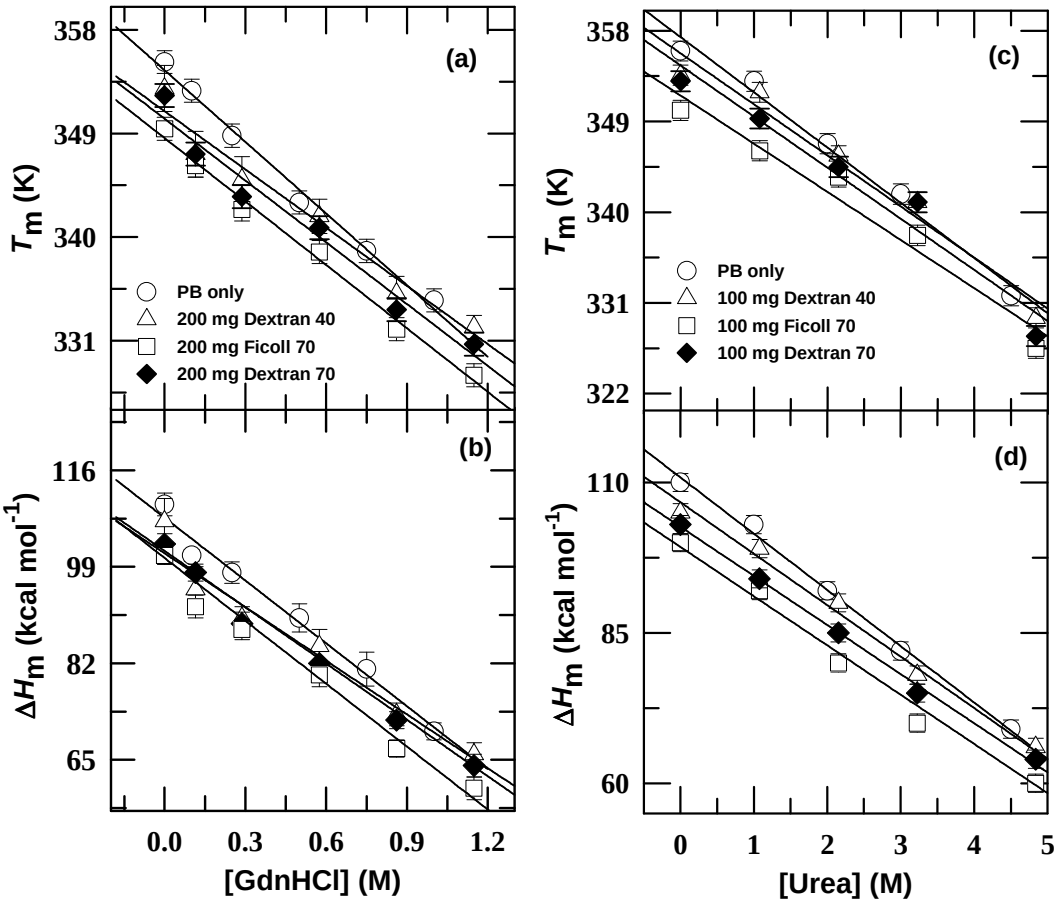
(a)
(b)
(c)
(d)
T_m (K)
ΔH_m (kcal mol^{-1})
PB only
200 mg Dextran 40
200 mg Ficoll 70
200 mg Dextran 70
100 mg Dextran 40
100 mg Ficoll 70
100 mg Dextran 70
[GdnHCl] (M)
[Urea] (M)

Fig. 10

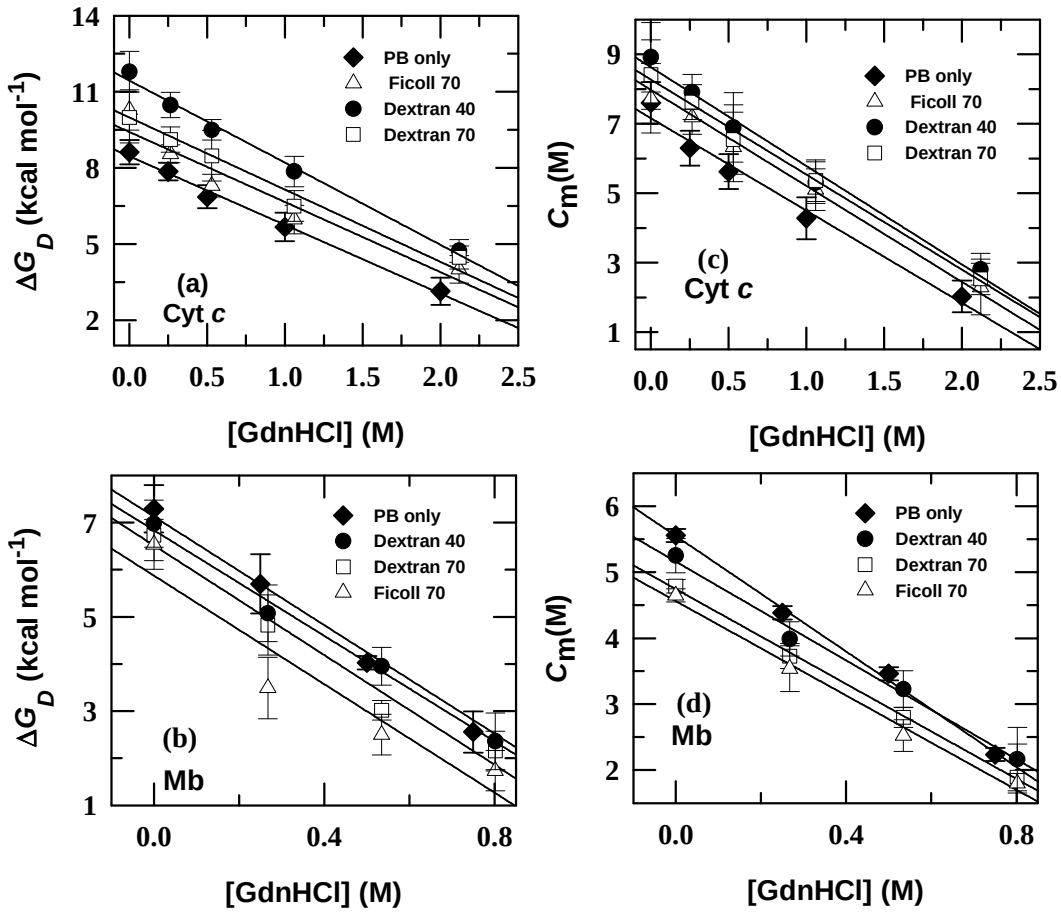
ΔG_D (kcal mol^-1)
PB only
Ficoll 70
Dextran 40
Dextran 70
(a)
Cyt c
[GdnHCl] (M)
C_m(M)
(c)
Cyt c
(b)
Mb
(d)
Mb

Fig. 11

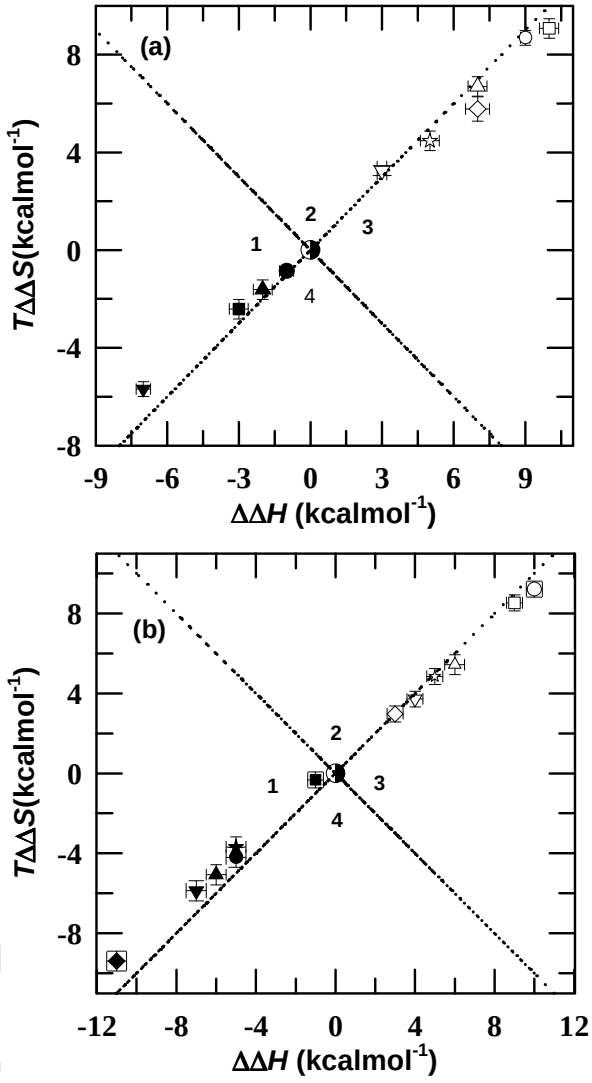
(a)
8
4
0
-4
-8
-9
-6
-3
0
3
6
9
TΔΔS(kcalmol-1)
ΔΔH (kcalmol-1)
1
2
3
4
(b)
8
4
0
-4
-8
-12
-8
-4
0
4
8
12
TΔΔS(kcalmol-1)
ΔΔH (kcalmol-1)
1
2
3
4

Supporting Information for

Factors Defining the Effects of Macromolecular Crowding on Internal Dynamics and Thermodynamic Stability of Heme Proteins *In-vitro*

Authors:

Rajesh Kumar[‡], Deepak Sharma[†], Vinay Kumar[□] and Rajesh Kumar*[††‡]

Authors' Addresses:

[††] Department of Chemical Sciences, School of Bassic and Applied Sciences, Central University of Punjab, Bathinda, 151001, India

[‡]School of Chemistry and Biochemistry, Thapar University, Patiala 147004, India

[†]Council of Scientific and Industrial Research—Institute of Microbial Technology, Sector 39A, Chandigarh, India

[□] Department of Plant Sciences, School of Bassic and Applied Sciences, Central University of Punjab, Bathinda, 151001, India

Corresponding Authors at:

Department of Chemical Sciences, School of Bassic and Applied Sciences,

Central University of Punjab, Bathinda, 151001, India

School of Chemistry and Biochemistry, Thapar Institute of Enginnering and Technology University

Patiala, 147004, India

Email: rajeshchem01@gmail.com

Phone: 91-164-286-4255

Table S1. Effect of crowding agents on [GdnHCl]-dependent ΔH_m, T_m and ΔC_p of Ferrocyt *c* at pH 7 as monitored by visible absorbance at 416 nm*.

without crowding agents				100 mg ml^{-1} ficoll 70				100 mg ml^{-1} dextran 70			
[GdnHCl] (M)	T_m	ΔH_m	ΔC_p	[GdnHCl] (M)	T_m	ΔH_m	ΔC_p	[GdnHCl] (M)	T_m	ΔH_m	ΔC_p
0.0	373.3	100	1.5	0.0	374.0	109	1.4	0.0	-	-	
0.25	372.4	92	1.4	0.27	372.5	101	1.5	0.27	372.3	105	1.4
0.5	366.8	80	1.4	0.53	368.9	94	1.5	0.53	370.1	100	1.4
1.0	362.8	75	1.4	1.07	364.7	85	1.4	1.07	365.1	90	1.4
1.5	358.8	70	1.5	1.60	359.9	78	1.4	1.60	360.4	78	1.4
2.3	350.7	60	1.5	2.46	353.4	70	1.5	2.46	355.7	71	1.4
2.8	348.7	55	1.4	2.99	347.6	63	1.5	2.98	351.8	62	1.4
100 mg ml^{-1} dextran 40				200 mg ml^{-1} dextran 70				300 mg ml^{-1} dextran 70			
[GdnHCl] (M)	T_m	ΔH_m	ΔC_p	[GdnHCl](M)	T_m	ΔH_m	ΔC_p	[GdnHCl] (M)	T_m	ΔH_m	ΔC_p
0.0	375.2	114	1.4	0.0	-	-	-	0.0	-	-	-
0.27	372.5	110	1.4	0.29	-	-	-	0.31	-	-	-
0.53	370.4	103	1.4	0.57	371.3	107	1.4	0.62	374.0	115	1.4
1.07	365.7	104	1.5	1.15	369.3	101	1.5	1.24	371.8	108	1.4
1.60	361.5	95	1.4	1.72	366.4	92	1.5	1.86	366.0	97	1.4
2.46	355.8	87	1.4	2.64	358.9	83	1.4	2.86	361.5	89	1.5
2.98	352.0	76	1.4	3.22	352.5	73	1.4	3.48	357.4	74	1.4

*ΔH_m, T_m and ΔC_p are reported as kcal mol^{-1}, K, and kcal mol^{-1}K^{-1}, respectively. The uncertainties associated with ΔH_m, T_m and ΔC_p are ±1.5 kcal mol^{-1}, ±0.5 K, and ± 0.1 kcal mol^{-1}K^{-}respectively. GdnHCl concentrations mentioned in Table S1 are corrected for crowding agents using equations (4) and (4a).

Figure S1.

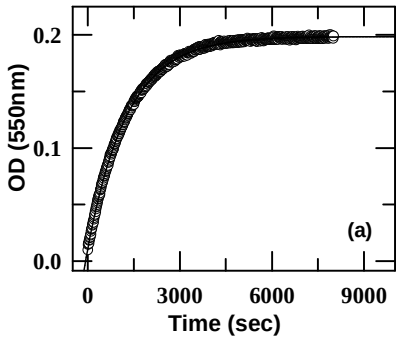

Figure S1. The slow single-phase dissociation of CO from NCO, NCO → N+CO (τ =32 min., 22°C). The NCO → N+CO reaction was probed at 550 nm in the presence of 0.05M GdnHCl, pH 7.0, 22 °C.

Figure S2.

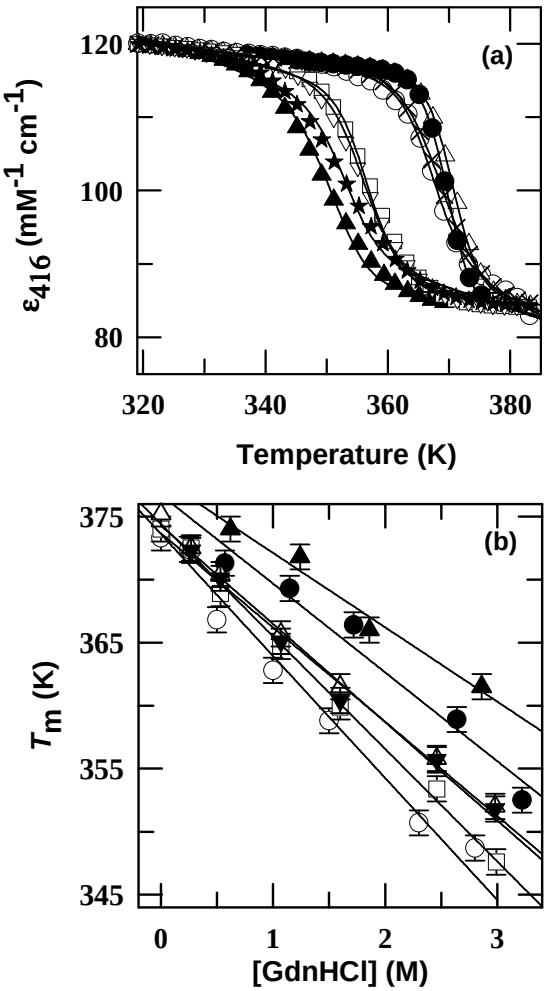

Figure S2. Effect of crowding agents on the denaturant-dependent thermal unfolding of Ferrocyt *c* at pH 7.0. Panel (a) represents the thermal denaturation curves of Ferrocyt *c* monitored at 416 nm as the change in absorption coefficient at 0.5 M GdnHCl (○), 0.5 M GdnHCl with 100 mg ml^{-1} dextran 40 (Δ), 0.5 M GdnHCl with 100 mg ml^{-1} dextran 70 (●), 0.5 M GdnHCl with 100 mg ml^{-1} ficoll 70 (×), 2.3 M GdnHCl (▲), 2.3 M GdnHCl with 100 mg ml^{-1} dextran 40 (□), 2.3 M GdnHCl with 100 mg ml^{-1} ficoll 70 (★), 2.3 GdnHCl with 100 mg ml^{-1} dextran 70 (▽). The solid curves in panel

represent nonlinear least-squares fits to equation (2) [82, 85]. Panel (b) shows the variations in T_m for Ferrocyt *c* (absorbance 416 nm) as the function of [GdnHCl] in the absence (○) and presence of 100 mg ml^{-1} (dextran 40 (Δ), dextran70 (▼), ficoll70 (□)), 200 mg ml^{-1} of dextran 70 (●) and 300 mg ml^{-1} of dextran 70 (▲) at pH 7.0. The parameters are summarized in Table S1 (absorbance 416 nm). The solid lines in panel (b) represent linear least-squares fit of the data.

Figure S3.

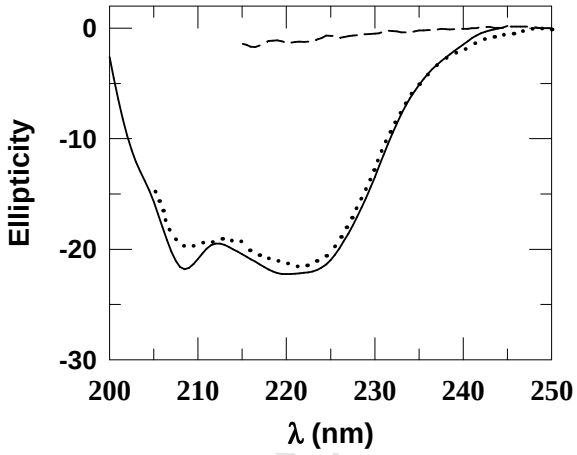

Figure S3. Far-UV CD spectra for the different states of ferrocyt *c* collected 25 °C. Far-UV CD for the native Ferrocyt *c* (N-state (solid line)), NCO-state (dotted line) and UCO-state (short dash line). The Far-UV CD spectrum of UCO is not collected below 210 nm due to an elevation of the HT voltage; especially, peptide signals are increasingly obscured with high GdnHCl content.

Figure S4.

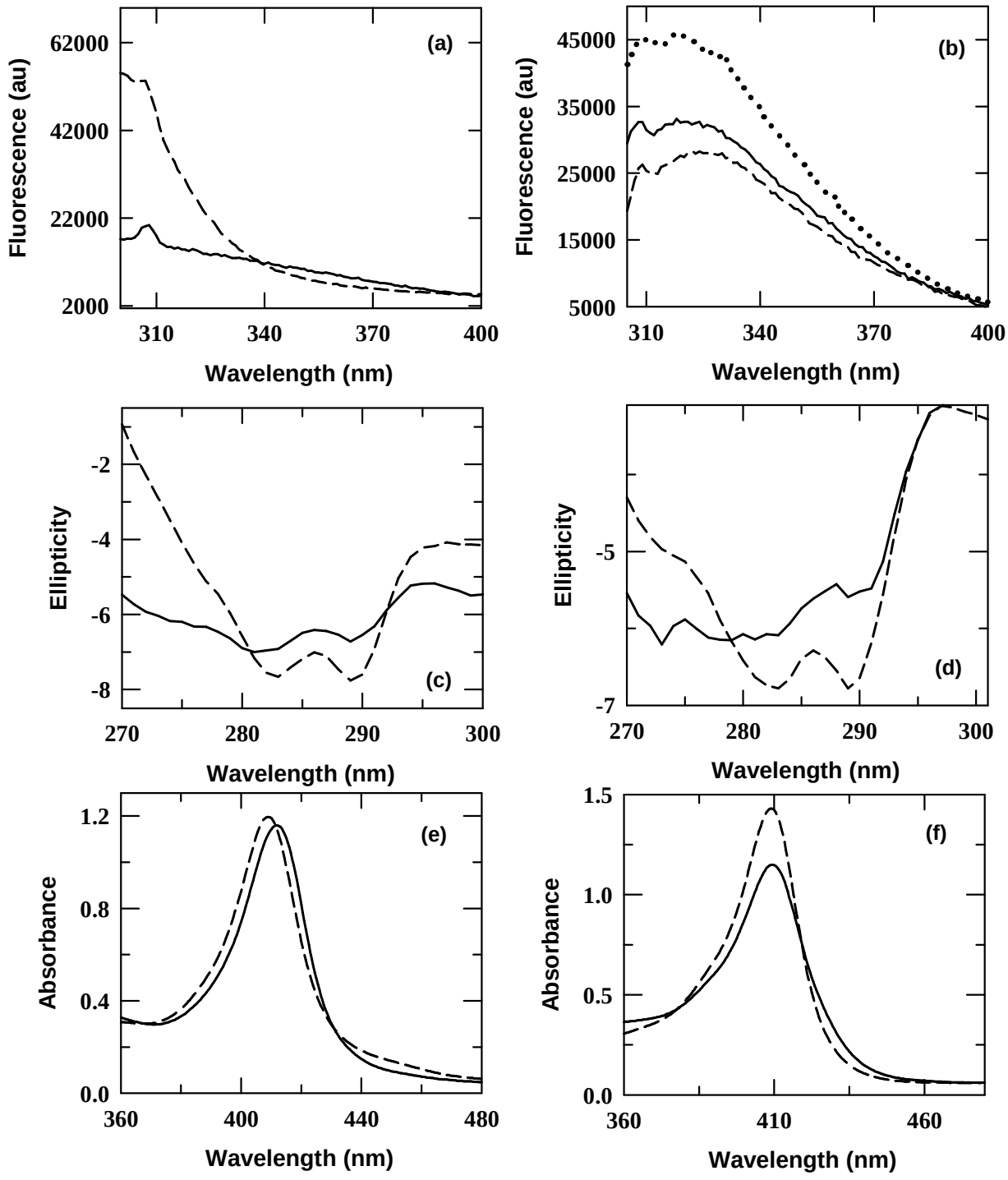

Figure S4. Panels (a) and (b) present the tryptophan fluorescence emission spectra native Ferricyt *c* and Mb, respectively, collected in the absence (short dash line) and presence of ~ 100 mg ml^{-1} ficoll 70 (solid line) at pH 7.0, 25 °C. Panel (b) also present the tryptophan fluorescence emission spectra native Mb collected in the presence of ~ 300 mg ml^{-1} ficoll 70 (dotted line) at pH 7.0, 25 °C. Panels (c) and (d) present the near-UV CD spectra native Ferricyt *c* and Mb, respectively, collected in the absence (short dash line) and presence of ~ 100 mg ml^{-1} ficoll 70 (solid line) at pH 7.0, 25 °C. Panels (e) and (f) show the near-UV CD spectra native Ferricyt *c* and Mb, respectively, collected in the absence (short dash line) and presence of ~ 100 mg ml^{-1} ficoll 70 (solid line) at pH 7.0, 25 °C

Highlights-

►Low concentrations of denaturants restrict dynamics of NCO and MbCO.
►Crowding presence opposes structural-fluctuation causing the unfolding.
►Size, shape and viscosity of crowders modulate the denaturant-mediated dynamics
►Crowding agent counteracts the destabilizing effect of denaturant for Cyt *c*
►Crowding agent enhances the destabilizing effect of denaturant for Mb